ABSTRACT

INVESTIGATING LOW-COST OPTICAL SPECTROSCOPY FOR SENSING
PRESSURE ULCERS

by Smruti Suresh Mirchandani

Diffuse Reflectance Spectroscopy has been used widely to characterize tissue properties for diagnostic and therapeutic applications. This thesis focuses on the use of spectroscopy for early pressure ulcer detection. The most common early diagnosis technique for pressure ulcers is a blanch test. A major issue with a blanch test is that it is purely visual and cannot be visibly observed on dark skinned individuals. Studies have already proven that spectroscopy can be used to detect blanch response in skin across light and dark skinned individuals. The portable reflectance spectroscopy setup showed that pressure changes to the skin can be detected spectroscopically. Some work on an iPhone based spectrometer was also done to have a low-cost spectroscopy alternative to the usual DRS equipment. This study failed to develop an iPhone based spectrometer but various factors that can be changed to better this research have been mentioned in this thesis.

INVESTIGATING LOW-COST OPTICAL SPECTROSCOPY FOR SENSING
PRESSURE ULCERS

A Master's Thesis

Submitted to the

Faculty of Miami University

in partial fulfillment of

the requirements for the degree of

Chemical Engineering

by

Smruti Suresh Mirchandani

Miami University

Oxford, Ohio

2017

Advisor: Dr. Karthik Vishwanath

Advisor: Dr. Jessica Sparks

Reader: Dr. Robert Applebaum

This Thesis titled

INVESTIGATING LOW-COST OPTICAL SPECTROSCOPY FOR SENSING
PRESSURE ULCERS

by

Smruti Suresh Mirchandani

has been approved for publication by

College of Engineering and Computing
and
Department of Chemical, Paper and Biomedical Engineering

_____
Dr. Karthik Vishwanath

_____
Dr. Jessica Sparks

_____
Dr. Robert Applebaum

TABLE OF CONTENTS

LIST OF FIGURES

ACKNOWLEDGEMENTS

Firstly, I would like to thank Dr. Karthik Vishwanath for giving me the opportunity to work on this research project. Thank you for all your guidance and feedback and patience with me when it came to learning something I have never done before. I would also like to thank Dr. Jessica Sparks for giving me the opportunity to work on this research and all the support throughout my entire time at Miami University. In addition, I would like to thank Dr. Robert Applebaum for being part of my thesis committee and for all the input and feedback into my research.

Lastly, I would like to thank my family. Thank you, Mom and Dad, for the tremendous amount of support throughout my entire education. I wouldn't have gotten this far without your encouragement, constant support and trust.

Chapter 1 INTRODUCTION

Pressure ulcers or bedsores are a serious concern in the elders. The most common early diagnosis technique currently is a visual blanch test. A visual blanch test involves applying gentle pressure to the test site for approximately five seconds and watching for the reperfusion of blood. Since stage I pressure ulcers are characterized as non-blanchable erythema, the nurses watch for risk areas where the skin will not blanch and a constant redness is observed even after pressure application. This way of testing puts dark skinned patients at a big disadvantage because a blanch test cannot be observed visually on darker skin tones. Diffuse Reflectance Spectroscopy (DRS) is a non-invasive technique that is widely used in therapeutic and diagnostic applications in the biomedical field[39-48]. A cost effective optical spectroscopy system seems promising for characterizing blanch response in skin and has already been successful in studies conducted previously [10,38].

Emerging new technology in the smartphone world has changed the perception of a smartphone as just a communication tool. By 2014, Ericcson reported 2.1 billion smartphone users in the world and this number is expected to grow three-fold by 2020[34]. Smartphones have advanced cameras, carry their own light source and do not require any external power to operate. Their ease of access also provides more motivation for them to be used in the biomedical field. Several papers have done work to develop smartphone based spectrometers[35-37]. A smartphone based spectrometer that can be geared towards early pressure ulcer diagnosis would provide ease of access in testing and diagnosing pressure ulcers in patients at nursing homes.

The main objective of this research is to develop an optical spectroscopy system to characterize blanch response in normal skin. This setup would provide a low-cost alternative in early pressure ulcer diagnosis. The second objective of this research is to develop a smartphone based spectrometer which can further be optimized to be used in early pressure ulcer diagnosis.

Chapter 2 PRESSURE ULCERS

2.1 Pressure Ulcers: Classification and Pathophysiology

Pressure ulcers are a serious healthcare concern for the elders. They are a serious cause of morbidity and immobility. The library of medicine describes pressure a pressure ulcer as "an ulceration caused by prolonged pressure on the skin and tissues when one stays in one position for a long period of time"[1]. The words pressure ulcer, bedsore or pressure sores are used synonymously. Ever since the 1970's there has been a continuing dilemma on what pressure ulcers should be called and how they should be classified. This also hampers the progress of moving towards the prevention and care of this condition.

The elders account for more than 60% of pressure ulcer patients and therefore are the largest risk group amongst the affected[2]. This is because the elders have a higher risk of suffering from diseases that lead to immobility such as stroke. The elders also go through changes in skin and blood vessels with progressing age, which combined with lesser position changes while sleeping or sitting makes them more prone to pressure ulcers [2].

Other general risk groups include patients that have suffered from Spinal Cord Injury, any other severe illnesses and/or multiple trauma. The priority in such cases is always given to securing proper functioning of vital organs and thus pressure ulcers are considered a secondary risk. The use of wheelchairs for such risk groups only heightens the risk of getting pressure ulcers[2].

Preterm infants present an entirely different risk group. The fact that their independent mobility and reflexes are not well developed at this stage makes them highly susceptible to pressure ulcers.

2.1.1 Pressure Ulcer Classification

EPUAP (European Pressure Ulcer Advisory Panel) and NPUAP (National Pressure Ulcer Advisory Panel) provide definitions that are used most widely in clinical practice.
The EPUAP defines a pressure ulcer as "an area of localized damage to the skin and underlying tissue caused by pressure, shear, friction and/or combination of these"[4].

The NPUAP defines a pressure ulcer as localized injury to the skin and/or underlying tissue usually over a bony prominence as a result of pressure in combination with shear and/or friction[5].

The EMBASE (Excerpta Medica Database) places all the categories of pressure ulcers under the term decubitus which belongs to a category of skin ulcers. The ICD-10 (International statistical Classification of diseases & Related Health Problems) also classifies all pressure ulcers as decubitus ulcers which is placed under the skin category[3].

Pressure ulcers are classified according to their clinical physical appearance. Two most popular classification systems come from the NPUAP and EPUAP. For the purposes of this research, the NPUAP classification system will be referenced and used. The NPUAP classification of pressure ulcers splits pressure ulcers according to their development in stages. Three stages of pressure ulcers are defined below [6].

Stage 1: This stage is defined by the skin still being intact with some redness in a localized area of bony prominence. The skin area might be painful, firm, soft, warmer or cooler when compared to adjacent tissue [6]. This stage is usually hard to detect in individuals with darker skin tones.

Stage 2: This stage is the onset of the "bed sore" or the wound. A shallow open ulcer with a pink-red wound is observed. Typically presents as a dry shallow ulcer without any bruising. If bruising does exist, then a deep tissue injury is suspected.

Stage 3: This is the final stage whereby full thickness tissue loss has occurred. Some of the sub-cutaneous fat may be exposed but the tendon, muscle or the bone still remain unexposed. The depth of tissue loss is highly dependent on the location of the pressure ulcer. Some areas do not contain subcutaneous tissue and therefore Stage 3 ulcers in these areas can still be shallow. Areas with more fat tissue are more likely to carry deeper ulcer wounds [6].

Stage 4: At this stage, full thickness tissue loss occurs with a possibility of exposing the bone, tendon or muscle. As with stage 3, the depth of tissue loss is dependent on the location of the pressure ulcer. Areas with no subcutaneous tissue will always present shallow ulcers. Stage 4

ulcers typically extend into muscle and/or supporting structures which presents a possibility of osteomyelitis [6].

Following stage 4, the pressure ulcers are deemed as a deep tissue injury and further described as unstageable by the NPUAP.

Suspected deep tissue injury: Purple or maroon localized area of discolored intact skin or blood-filled blister due to damage of underlying soft tissue from pressure and/or shear. The area may be preceded by tissue that is painful, firm, mushy, boggy, warmer, or cooler as compared to adjacent tissue. Deep tissue injury may be difficult to detect in individuals with dark skin tones. Evolution may include a thin blister over a dark wound bed. The wound may further evolve and become covered by thin eschar. Evolution may be rapid, exposing additional layers of tissue even with optimal treatment [6].

Unstageable: This is when full thickness tissue loss has occurred and the ulcer is covered by extreme amounts of slough or eschar. True depth of the wound cannot be determined because the base of the wound is not exposed. All slough and eschar needs to be removed to expose true depth of the wound. This is what makes the pressure ulcer unstageable.

2.1.2 Pressure Ulcers: Pathophysiology

From the existing definitions of pressure ulcers, the following factors play a key role in pressure ulcer development.

2.1.2.1 *Pressure*

Immobility induces great pressure on the tissues between the surface and bony areas. Four major theories of tissue breakdown due to pressure ulcers are discussed below.
Ischemia caused by capillary occlusion: Increased pressure leads to capillary occlusion which causes ischemia (inadequate supply of blood to the specific area). Ischemia not only changes membrane permeability in capillaries but also enhances the chances of inflammatory reactions [6].

Reperfusion Injury: Reperfusion of blood after ischemia causes cellular edema, tissue damage and over production of reactive oxygen which triggers a process called oxidative stress. This leads to an accumulation of unfolded proteins which in turn cause ER stress. In compressed regions, when muscle tissues go through this phenomena, they become a site for Deep Tissue Injury (DTI) [7]. A DTI is a severe form of pressure ulcer where tissue damage starts in subcutaneous tissue layers, under intact skin [5].

Lymphatic function is impaired: Increased pressure reduces blood supply in the affected area which leads to a condition known as hypoxia. Hypoxia is a condition whereby tissues do not receive sufficient oxygen. This damages the lymphatic vessels and impairs lymph flow. This eventually leads to tissue necrosis (death of cells in tissue) [6].

Pressure induced injuries always start in muscle and/or subcutaneous fat and are visible on the skin later only due to the fact that skin can survive longer periods of ischemia without irreversible damage [6].

2.1.2.2 *Shear*

Shear and pressure both exert forces on the tissue and often a firm distinction between the two is hardly possible because pressure causes shear and shear causes compressive forces in the tissue. Shear acts similarly to pressure as stated above and the mechanisms that cause pressure ulcers due to shear are tissue distortion, pinching and occlusion of capillaries, reductions in blood flow and physical disruption of tissues and blood vessels[8].

Tissues are not homogenous and comprise of different layers with different mechanical properties. Shear stresses can cause relative movement of one layer over the other. The extent of movement (physical disruption and vessel occlusion) is affected by factors like the elasticity and stiffness of tissue layers. Hence, in aged groups there is a higher prevalence of pressure ulcers because of the reduced elasticity between the tissue layers. Stiffer tissues tend to deform lesser than tissues with lower stiffness. The greatest potential for shear stresses lies between the bone and muscle, muscle and fat tissue and finally between tissues and fat tissues. This is why interface pressures are highest at bony prominences and people with prominent bones are more prone to higher shear and pressure [8].

2.1.2.3 *Friction*

Friction is found to be more damaging on superficial tissue layers, whereas the deeper tissue layers stay intact. Pressure and shear are usually seen as main causes of pressure ulcer formation, but this is only true when the damage is in the deeper tissue layers, while superficial skin lesions are caused by friction. Pressure and shear are not considered contributing causes to superficial skin lesions [6]. A superficial ulceration occurs when a small pressure with a large tangential force is applied to the skin. Skin that is already irritated or inflamed is prone to superficial lesions due to friction [8].

2.2 Current Diagnosis

Pressure ulcers are diagnosed according to the NPUAP staging. Currently pressure ulcers are detected via a clinical visual examination. Pressure ulcer checks are usually done on at risk patients as described in the section above. A pressure ulcer check is done by checking for noticeable different pigmentation on the skin. Typical areas such as back of the head, shoulder blades, elbows, buttocks, tailbone and heels are always examined first in patients with limited mobility. A skin color change to red, blue or purple in the suspicious areas is usually the first visual sign of pressure ulcers.

After a visual diagnosis, ultrasounds and blood tests may be needed to aid in staging the ulcer correctly. Tissue cultures to check for a bacterial or fungal infection may also be necessary [9].

2.3 Current Technologies for PU detection

2.3.1 Laser Doppler Flowmetry

This is a measure of blood flow. A Helium Neon laser source is used to transfer light to the tissue via optical fibers probes and a second probe is used to collect the light backscattered from the tissue. The Doppler effect detects the movement of red blood cells in blood. This technique helps provide information on superficial tissue layers. Laser Doppler Flowmetry (LDF), then measures a quantity called flux which is a function of red blood cells and their velocity. LDF has been used extensively to characterize the differences between pressure damaged and normal tissues.

LDF, however, does have a degree of background noise whereby a flux has been recorded even when there is no blood flow in the tissue. Moreover, the flux measurement is a function of movement of all the different vessels and the source of movement is never known. It is also highly variable with time and location [10].

2.3.2 Transcutaneous Oxygen Monitoring (TCPO$_2$)

This technique is used to measure the O$_2$ content in blood in a tissue. A chamber is attached to the skin using an adhesive ring. A solution is placed in the chamber and a transcutaneous probe connects the chamber to a monitoring device. The probe heats the skin up to a temperature of 45 °C. This makes the skin more permeable to oxygen diffusion, dissociation and it brings more oxygen containing blood to the sampling region. The gas then emerges from the tissue and an electrochemical reaction takes place in the chamber which is then measured by the probe. TCPO$_2$ measurements have been used to characterize the oxygen content in damaged versus healthy tissues.

This technique does require at least 15-20 minutes of stabilization, after each recording, to obtain accurate measurements. A major concern is also the burns to the skin during this test. Pressure Ulcer patients are more susceptible to burns from the chamber due to the tissue already being damaged. The measurements can also be easily influenced by the environment and therefore it requires a lot of control during the tests [10].

2.3.3 Ultrasound Imaging

Ultrasound imaging creates a cross sectional image of the area being examined. The image is obtained by placing a transducer in contact with the skin along with a coupling medium (such as gel). The transducer converts electrical energy to sound waves. The sound waves entering the specific area are absorbed, reflected or scattered by tissues. The sound waves are reflected and converted to electrical signals that are displayed on a screen. Abnormal tissue can be identified by the differences in density of certain tissue areas. High frequency ultrasound has been used to assess skin wounds and is a valuable assessment tool in staging pressure ulcers [10].

However, imaging a PU wound with ultrasound can be difficult due to the shape of the wound. Moreover, the skin hydration by the gel can change the properties of the wound.

2.4 Novel Early Detection Strategies

2.4.1 Portable Gage

This is a novel handheld instrument that is designed to detect a change in skin's biomechanical properties by measuring its biomechanical response. It can be used to detect stage I pressure ulcers and deep tissue injuries [11].
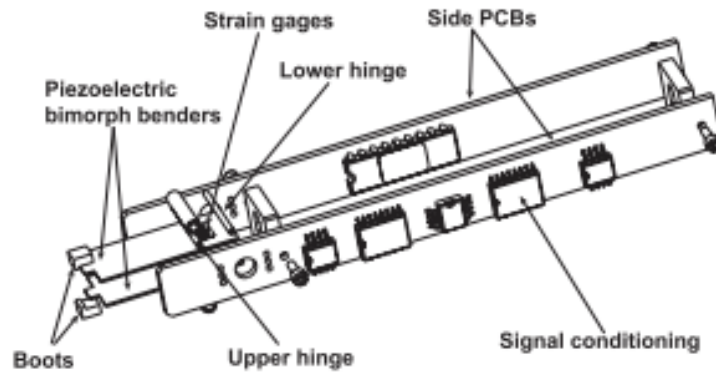
Figure 2-1: The pressure ulcer gage[11]

The design consists of two bimorph piezoelectric benders that are arranged such as to achieve large skin strains. The developers conducted a quasi static stretch test with the device, where a ramp voltage from -90 V to 90 V was applied to the benders. A stretch force vs voltage and a stretch force vs strain response was recorded. The device successfully showed that the elasticity and viscoelasticity of different types of skin was significantly different[11].

2.4.2 Bioimpedance spectrometer

A portable bioimpedance spectrometer that detects subtle changes in the electrical properties of tissues. The device consists of four electrodes that are placed on the tissue surface. Two of the electrodes are used to inject current into the tissue and the other two measure the voltage on tissue impedance. This device has a wide frequency range, little power consumption and is low

cost. The main objective of this device development is for it to be used clinically in the risk assessment of pressure ulcers in the future [12].

2.4.3 SEM (Sub Epidermal Moisture) scanner

SEM is a biophysical measure that assesses the epidermal barrier function of skin [13]. It can be measured by measuring the surface electrical capacitance. The surface electrical capacitance is calculated from the impedance of skin to electrical forces, and directly relates to any edema in the epidermal or sub-epidermal layers of skin. Prior studies have already made use of SEM measures to evaluate wound healing and found that tissue edema levels can be used as markers to assess wound healing. SEM is useful in identifying minor skin damage and has been able to predict stage I pressure ulcers a week prior to their occurrence [13]. SEM has been proven as a successful tool to predict early stages of pressure ulcers and thus allows for early prevention strategies to be put in place.

The SEM scanner is a medical device used by a lot of healthcare providers as a part of the pressure ulcer prevention program [14]. Clendenin *et al.* tested the device's reliability and concluded that the device is in fact highly reliable and stands in good agreement across various operators and different devices. This study was based on inter-device agreement of the SEM scanner and it proved the scanner to be a reliable method of predicting early pressure ulcer damage.

2.4.4 Smart Bandage

The Smart Bandage is yet another impedance sensing device, which makes use of impedance spectroscopy to detect early tissue damage due to pressure. The device has an array of electrodes and some control hardware that is responsible for performing impedance spectroscopy across the electrodes. The design consists of a compact printed circuit board with gold plated electrodes. Impedance spectroscopy has been correlated to tissue health and identifies tissue damage that is not visible yet. Wounded areas have been proven to show lower impedance with more conductivity and lesser capacitance. These qualitative observations are consistent with a loss in cell membrane integrity. Mild reversible pressure damage was used to test whether impedance

truly detects pressure damage before any visible damage. The impedance sensor detected lower values and damaged tissue in the regions of induced pressure [15].
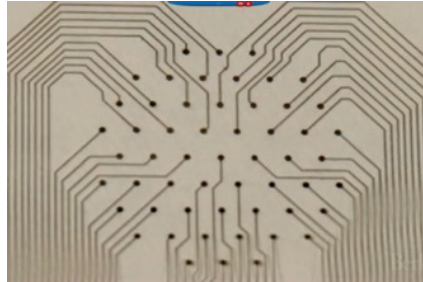
Figure 2-2: Smart Bandage[15]

2.4.5 Diffuse Reflectance Spectroscopy

Diffuse Reflectance Spectroscopy (DRS) is a non-invasive method that uses light reflected from the skin to obtain information about the type and concentration of biochemical substances in the skin tissue such as melanin and hemoglobin [10]. The spectroscopy of tissues involves measuring the attenuation of the light intensity by the tissue relative to the incident light [16]. Tissue optics can help in choosing optimal treatment procedures, staging the wound and studying the therapeutic responses during the healing process [17]. DRS has been used to characterize normal and malignant states of different tissues such as colon, oesophagus, oral cavity, cervix, ovary and breasts [17]. More specifically NIR spectroscopy is used to obtain information on hemoglobin (HbO_2), deoxyhemoglobin (Hb) and tissue hydration levels, which in turn help in characterizing damaged and normal tissues [16].

Tissue reflectance is measured with instrumentation that involves fiber optics, a light source (typically halogen) and a spectrophotometer. Light in the visible wavelength range (400 to 700 nm) is used because it is considered to be the least harmful in the sense of causing any thermal injury to the skin. The spectrophotometer converts photons into electrical signals that are a function of the amount of light (intensity) reaching the detector and the duration of the exposure [10].

The absorbance of the light from the tissue is calculated by a quantity known as the Log Inverse Reflectance (LIR). This is calculated by taking the log of the ratio of the diffusely reflected light

from the tissue and the light reflected from a white surface (standard). The absorbance of light at various wavelengths has been used to create various trends for different skin pigmentations and to characterize various tissues as mentioned above.

Stranc *et al.* conducted a study on nine rats using NIR spectroscopy to assess tissue viability. Quantities such as tissue hydration, hemoglobin and oxyhemoglobin saturations of the tissue were monitored. This paper concluded that tissue viability could indeed be assessed by NIR spectroscopy.

2.5 Pressure Ulcer Prevention

Since pressure ulcers are not only hard to detect but also difficult to treat, certain key preventative principles should always be put in use in order minimize the occurrence of pressure ulcers as much as possible. The key preventative principles are risk minimization, pressure reduction, avoidance of skin damage, avoidance of maceration (softening or breaking down of skin), promotion of movement and nutrition.

2.5.1 Risk Minimization

Risk minimization is one of the most obvious preventative measures. Identify risk groups such as elders patients with limited movement, wheelchair bound patients and/or patients that are bed bound due to trauma. Regular skin inspection of risk groups by trained professionals along with regular updates on the patients' mobility should be conducted so that any early onset of ulcers can either be identified at its earliest or it can be prevented. Other major factors like keeping the patient on a steady treatment plan and monitoring high risk patients closely will help identify any risk factors that might contribute to pressure ulcers[2].

2.5.2 Pressure Reduction

Pressure is known to be one of the major causes of pressure ulcers. Pressure reduction through change of positions regularly, pressure distribution and reduction of pressure on bony prominences is important to aid in reducing the risk of pressure ulcers. The change of positions is done by putting each patient on his/hers individualized patient positioning plan where the positions are changed regularly to reduce pressure over certain areas.

Chapter 3 DIFFUSE REFLECTANCE SPECTROSCOPY

3.1 Background

Optical methods have gained a great amount of importance in disease diagnostics over recent years. Many reports have been published over the last two decades describing the use of DRS in vivo to provide a noninvasive ''optical biopsy'' of many different organ sites including the breast, esophagus, bronchus, brain, pancreas, GI tract, and cervix to characterize pre-cancers and cancers in these tissues[39-48]. Diffuse reflectance works on the principle of guiding light beam into the sample where it is scattered, reflected and transmitted through the sample. The back reflected light is then collected and guided to detector optics [18]. This produces a spectrum that contains information about the sample. The spectrum is a signal that is based on the amount of light scattering and being absorbed in the sample [19]. Diffuse Reflectance Spectroscopy (DRS) has applications in a multitude of areas like color measurement of textiles, pharmaceuticals, building materials, paper and pulp and in other investigations in physical, organic and inorganic chemistry [20].

One of the major applications of DRS are for determining tissue properties. DRS probes the absorption and scattering properties of the skin [21]. DRS in the visible wavelength range is sensitive to the absorption and scattering properties of epithelial tissue. This is a non-invasive method that shows promise as use for a lot of early detection of diseases [22,23]. A basic setup for a DRS system is shown in Figure 1 [19]. A basic setup consists of a spectrometer, fiber optics to guide the light to and from the skin and a detector which is usually a laptop/computer.
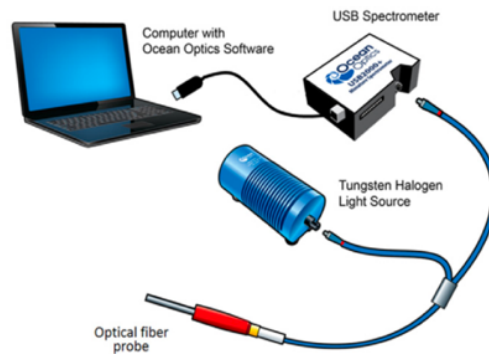
Figure 3-1: A schematic of the basic DRS setup [19]

3.2 The optics of human skin

The human skin consists of multiple layers. It can be subdivided into two major layers, namely the epidermis and dermis. The epidermis consists of eight sublayers with the stratum corneum being the top most layer. Every layer has different inherent optical properties due to the changes in chromophores such as melanin, blood and keratin [24].

The optics of normal skin are schematized in Figure 2. For normally incident radiation about to 4% to 7% of the beam is reflected. This is known as regular reflectance and occurs over the entire spectrum (250 nm – 3000 nm) [25]. The skin does not have any specular reflection due to the roughness of the stratum corneum and the refractive index of the skin. The difference in refractive indexes of the air and tissue also cause internal reflection of the back scattered radiation. The amount of incident radiation that is not returned as regular refraction is absorbed or scattered. Absorption and scattering determine the penetration of radiation into the skin and the reflection of scattered radiation from the skin [25]. Scattering of light occurs due to inconsistencies in the medium's refractive index. Inconsistencies in the medium's refractive index exist due to physical inconsistencies. Scattering occurs in different spatial distributions and intensities, depending upon the size and shape of the inconsistencies compared to the wavelength. For example, molecules that are much smaller than the wavelength (one tenth of the magnitude of the wavelength or smaller), produce weak and well distributed scattering. Similarly, the scattering due to collagen fibers is of great importance when determining the penetration of incident radiation in the dermis[25].

Figure 3-2: Optical pathways in skin[25]

13

The stratum corneum and epidermis usually have high absorbance due to the presence of peptide bonds. The absorption spectra of various epidermal chromophores such as DNA, urocanic acid, DOPA-melanin, tryptophane and tyrosine is responsible for corneal or epidermal transmittance in the UV region. The individual and anatomic variations in the epidermal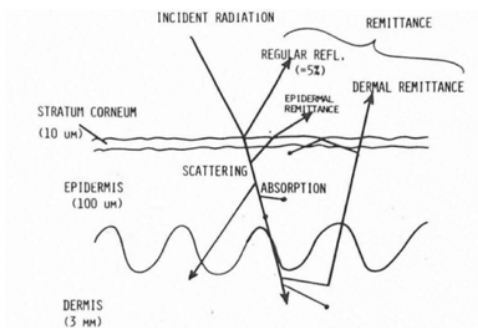 transmission are largely due to the variations in the concentration, distributions or amounts of these chromophores[25]. The scratum corneum and epidermis play the role of an optical barrier by absorption of incident radiation. Melanin, is the major absorber of radiation in the 350 nm – 1200 nm wavelength region. Hemoglobin, oxy-hemoglobin, beta-carotene and bilirubin are the major absorbers of visible radiation in the dermis [25]. The penetration of optical radiation in human skin is highly wavelength dependent. Melanin and hemoglobin are the main chromophores of human skin in the visible range. Melanin exists in the epidermis in the top 50 μm – 100 μm and hemoglobin is found further deeper in the skin about 50μm – 500μm[21] below the surface, in the dermis.

Light transport through tissues is described using the scattering coefficient, absorption coefficient and the anisotropy factor [26].

3.3 Mathematical models to characterize tissue optics

The ability of light to penetrate a tissue, interact with the tissue components and then reflect, is key to diagnostic applications. Characterizing the optical properties of tissue aids in designing devices and interpreting measurements [27]. Melanin, beta-carotene and oxygenated and deoxygenated hemoglobin are largely responsible for the absorption of visible light in human skin. Collagen and sub-cellular organelles are responsible for the scattering of visible light[28]. A lot of research exists on the methods and models to quantify tissue spectra. These models are mathematically and computationally intensive, therefore a brief overview of the most common models is discussed briefly below.

3.3.1 Monte Carlo

Monte carlo function uses a probability density function that involves a scattering coefficient to

14

obtain the distance travelled by the photon along an optical path. The absorption is modelled by assuming all photons have a weight of one while entering the tissue and then taking this value and attenuating it according to the Beer Lambert law [28]. The Beer Lambert law states that the absorbance and concentration of the absorbing species are linearly proportional. Monte carlo simulations for reflectance are run for one wavelength at a time due the wavelength dependency of the absorption coefficient, the scattering coefficient and the anisotropy.

3.3.2 Diffusion Approximation (DA)

This model is employed for simple geometries and assumes that the absorption of light in the tissue is negligible compared to the scattering. Zonios *et al*., used DA to model diffuse reflectance from the skin and obtained hemoglobin and melanin concentrations in vivo [21]. The model was also used to measure the absorption and scattering coefficient of the skin. The scattering properties of the skin, melanin concentration and the melanin content were found to be consistent with measurements made in other reports at the time. Georgakoudi *et al*., characterized the scattering properties of dysplastic and non-dysplastic Barret's Esophagus using the DA model. Ex vivo, the DA model was used by Ghosh *et al*., to approximate the absorption coefficients, scattering coefficients and the anisotropy factors for normal and malignant breast tissues. It was found that malignant breast tissue had a larger absorption and scattering coefficient in the visible wavelength range [31].

3.3.3 Look table based model

The Look Up Table (LUT) based algorithm is developed purely from a LUT that is generated from experimental measurements on tissue simulating phantoms and does not depend on any analytical or computational models. A look up table is generated by measuring the reflectance using tissue phantoms with known optical properties. The optical properties of any site of interest are then obtained by fitting the diffuse reflectance spectra of the said subject to the LUT using a non-linear optimization fitting technique. A lot of empirical models have also been developed for determining the optical properties of tissue through DRS but the biggest issue remains that these models are still specific to probe geometry and detector source separation [41,42].

3.4 Applications

DRS has a plethora of applications ranging from color matching and identification in textiles to characterizing and measuring mineral content in soils[20-22]. Over the past two decades, DRS has gained a lot of attention for the work done in the medical field. This paper will briefly discuss some applications in the medical field.

A lot of work has been done to prove that epithelial cancers such as cervical and oral cancers have a better chance of being treated with surgery, chemotherapy, radiation or a combination of above if detected early. In the presence of caner or pre- cancer stages in the tissue, the absorption, scattering and fluorescence properties undergo significant changes due to the changes in tissue composition, vasculature and metabolic function. Over the years DRS with the combination of appropriate mathematical models has become a highly useful form of extracting biologically relevant parameters for cancer detection [28]. Principle absorbers in the tissue such as oxy-hemoglobin, deoxy-hemoglobin, retinol and beta-carotene can be determined from the absorption coefficient.

Yu *et al.* made use of DRS to quantify and characterize pre-cancerous tissue in the cervix and oral cavity. DRS spectra was measured from the mucosal tissues of volunteers and a probe pressure sensitivity study was also conducted to characterize the effect of probe pressure on spectra acquisition. Properties such as total hemoglobin (THb), oxygenation (SO_2), absorption coefficients and scattering coefficients were used to characterize epithelial tissue. The absorption coefficients and scattering coefficients were computed using an inverse Monte Carlo model[32]. The oxygenation (SO_2), total hemoglobin (THb) and hemoglobin concentrations were computed from the absorption coefficient spectra with the help of Beer Lambert's Law.

Chang *et al.* used the DRS system along with inverse Monte Carlo modelling to characterize and quantify important optical biomarkers that change with different grades Cervical Intraepithelial Neoplasia (CIN) from normal cervical tissues. It was found that total hemoglobin (THb) was higher in high grade CIN when compared to lower grades of CIN [16].

16

Langhout *et al.* employed DRS and Fluorescence Spectroscopy (FS) to characterize colon cancer optically. Water content, fat content and hemoglobin concentration were used as the primary parameters to characterize and differentiate normal and malignant tissue[33].

DRS has also been widely used to characterize tumor tissue in breast, lung and liver tumors. reliable identification of tumor tissue and surrounding normal tissue has been reported for breast, lung, and liver tumors[17-19].

In recent years, a significant amount of work has also been done for the use of DRS in the field of diabetic foot ulcers. Anand *et al*. employed DRS to characterize foot ulcers using parameters such as total hemoglobin concentration and hemoglobin oxygen saturation. Foot ulcer diagnosis and wound healing is based purely on a clinical visual inspection[23]. This study proved DRS to be a useful tool in detecting changes in oxygen dynamics which is a valuable property in monitoring the ulcer wound healing process. DRS was proven to be effective in diagnosing foot ulcers by monitoring the oxygenation level in affected tissue sites.

3.5 DRS for the assessment of non-blanchable erythema

Pressure ulcers are a serious healthcare concern. They are a serious cause of morbidity and immobility. The library of medicine describes pressure a pressure ulcer as "an ulceration caused by prolonged pressure on the skin and tissues when one stays in one position for a long period of time"[24]. The words pressure ulcer, bedsore or pressure sores are used synonymously. Ever since the 1970's there has been a continuing dilemma on what pressure ulcers should be called and how they should be classified. This also hampers the progress of moving towards the prevention and care of this condition.

One of the most common methods of diagnosing a pressure ulcer is by conducting a visual blanch test. This is a test conducted in healthcare facilities to diagnose stage I pressure ulcers. The test is conducted by simply placing the finger over the site of inspection and applying gentle pressure for a period of five seconds. The pressure is then relieved and the capillary refill rate is observed visually by the naked eye. Stage I pressure ulcers are defined as non-blanchable erythema. This is a big concern for patients with dark pigmented skin because a visual blanch response is difficult to detect in darker skin tones[25,26]. Other methods for diagnosing early onset

of pressure ulcers is testing for skin temperature, consistency and temperature of the skin site in comparison to adjacent areas[27]. The problem lies with the lack of sufficient quantitative data to provide non-visual cues for early pressure ulcer detection. This coupled with the issue of skin color in pressure ulcer detection calls for a need of using optical methods to analyze and characterize tissues for early pressure ulcer detection.

The research for assessing a blanch response spectroscopically is recent. Matas *et al*. conducted a study where the focus was on characterizing blanch response spectroscopically with focus on eliminating the issue of skin color in blanch response assessment. The study induced pressure on the forearms of 10 light-skinned individuals and 10 dark skinned individuals with the use of a stepper motor with an attached probe. This was used to deliver controlled pressure to the participants' forearms Pressure readings were obtained every 0.5 seconds with the pressure increasing from 0mm Hg to 50 mm Hg and then being released. The maximum of 50 mm Hg was chosen such that it was greater than the pressure required to close capillaries in the forearm (30 mm Hg) while light contact with skin is defined at a pressure of 5 mm Hg[38]. This was defined as one blanch cycle. Six blanch cycles were performed on the subject and the data was acquired continuously. Visible and near-infrared spectra was analyzed. The study reported a significant change in the total hemoglobin (THb) in the tissue sites when pressure was applied. The total hemoglobin was significantly lower during the times of pressure application. This corresponds to less amount of blood present in the area when pressure is applied and therefore a lower THb is observed. The amount of melanin present during the blanch cycles was also calculated and it was found that no change in melanin concentration was seen in the forearms' in response to pressure. This helps in successfully separating the contribution of melanin in the measured reflected spectrum. This implies that any changes in the reflectance spectra were observed purely due to blood dynamics[28,29].

Another study in 2006, employed DRS to characterize blanch responses in light and dark skinned individuals. This study performed tests on the hell and sacrum of the test subjects. Data acquisition was not continuous and spectra was acquired at 1 spectrum per second. The probe was kept in light contact with the skin for 30 seconds and then a pressure of 120 mm Hg was induced through the indenter on the probe and was maintained for 30 seconds. It was found that there was a significant decrease in THb on the heels of light skinned and dark skinned patients

while the sacrum, did not show significant changes in THb and was considered inconclusive for the sacrum area[10]. The amount of THb change did not differ significantly within skin color groups. This proves that the data collection method around assessing a blanch response spectroscopically still needs a lot of work and exploration.

Chapter 4 A PORTABLE REFLECTANCE SPECTROSCOPY SYSTEM FOR MEASURING BLANCH RESPONSE IN NORMAL SKIN

4.1 Objectives

The main objective of this study was to assess the use of a portable reflectance spectroscopy for measuring blanch response in normal. The secondary objective of this study was to observe the effect of incremental pressure changes on normal skin.

4.2 Methods

4.2.1 Participants

This was a very small scale study and comprised of only four participants. Two of the participants were light skin males, while the other two participants were dark skin one male and one female. All participants fell in the 18-25 age group. The age group of the subject population was kept within the 18-25 age range to ensure that age did not become another variable factor in assessing pressure application to the skin.

All experimental procedures, risks, and benefits were discussed and informed consent provided prior to the beginning of any experimental procedures in compliance with the policies of the Institutional Review Board at Miami University.

4.2.2 Instrumentation

Figure 4-1 shows the instrumentation for this setup. The skin reflectance data was collected using a USB 4000 Ocean Optics spectrometer (c) in conjunction with a Tungsten Halogen light source (b). A 600 μm bifurcated reflectance probe (e) was used to guide light to site of interest and collect back scattered light from the skin site respectively. A laptop with Spectrasuite spectroscopy software (d) was used as the detector to analyze the reflectance data. The fiber probe was mounted on a fiber optic holder and two posts were attached on either side of the holder (a). Pressure was applied by hanging disc weights on both sides of the holder.

Figure 4-4-1: Experimental setup for spectroscopic blanch response assessment

4.2.3 Procedures

This study was designed to simulate a blanch response on normal skin. The pressure required to close capillaries in the forearm is 30 mmHg[38]. Five pressure levels ranging from 20 mmHg to 30 mmHg were induced on the sites to study the effect of increasing pressure on normal skin. The pressures were induced by hanging the appropriate amount of disc weights from the posts of the fiber optic holder. Measurements were taken from two sites on the back of the forearm. The light source was turned on at least 10 minutes prior to any testing to allow for it to warm up. Data was acquired as six different sets of measurements at each site. Thirty files were collected at each pressure level and the data acquisition rate was one file per second. Baseline data was collected with no weights as 0 mmHg. Thereafter, weights were added and the pressure was increased from 20 mmHg to 60 mmHg in 10 mmHg increments. and Describe the entire experimental setup with images and the calculations made. Data from a reflectance standard was collected before and after simulating all six pressure levels on a site to aid in the calculation of absorbance.

4.3 Results and Discussion

All raw data was converted to absorbance using the equation mentioned in Chapter 3. The raw data is presented in Figure 4-2 as an illustration. Figure 4-2 shows the base level (no pressure) data along with the five pressure levels. As one can see, there is some banding within the 30 acquired measurements at each pressure level, even though all six pressure levels cannot be distinguished clearly. However, when looked at closely in the 450 nm- 600 nm region, one can

differentiate the 0 mmHg data from 60 mmHg. When all the data at each pressure level is averaged and subsequently plotted, the treend seen in Figure 4-3 is observed.
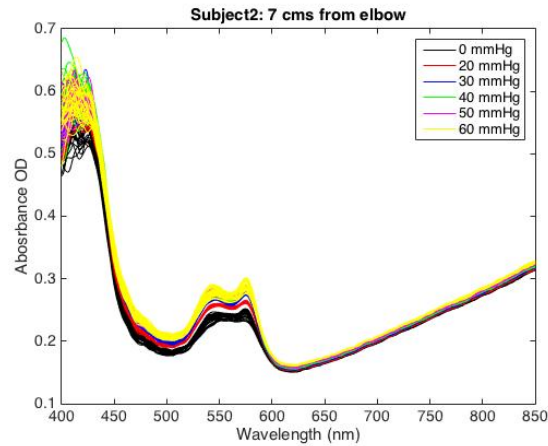

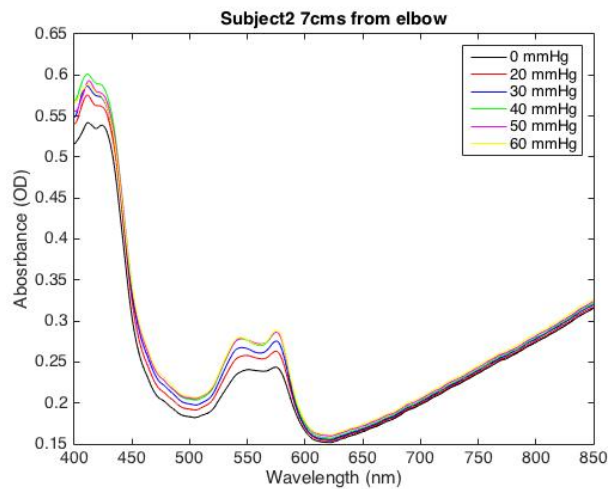*Figure 4-2: Absorbance at all pressure levels for Subject 2: 7 cm from the elbow*

Figure 4-3: Averaged Absorbance at all pressure levels for Subject 2: 7 cm from the elbow

The absorbance increases with an increase in pressure applied. This was not what was expected from the study. Increasing pressure on the skin displaces the blood in the tissue, this is what causes the skin to blanch, and with a lack of major chromophores in that area it would imply that the absorbance would decrease with increasing pressure[10,38]. For this experiment, the absorbance at any pressure level was found to be higher than the absorbance at base level. The reason for this phenomenon can be found by looking closely at the instrumentation, specifically the fiber optic holder. The fiber optic holder is an inch in diameter while the fiber optic is housed in the

center of the holder and has a collection fiber diameter of 600 μm. The sensing volume for this fiber optic is very small, hardly a millimeter into the skin. Considering the size of the disk that holds the fiber optic and the diameter and the sensing volume of the fiber optic, it was found that while inducing pressure on the skin using the weights the blood was being displaced from the edges of the disk to everywhere else, including the center of the disk where it made its way into the sensing volume of the fiber. Therefore, at higher pressures the absorbance was higher than that at the base level.

ANOVA (Analysis of variance) is a statistical technique used for detecting the difference in population means or whether the means of different groups are all equal when there are more than two populations[49]. This technique would be useful in testing whether the difference between the mean absorbance at different pressure levels is significantly different. This statistical technique tests a null hypothesis (H_0) which states that all population means are equal. The null hypothesis for this study was that mean absorbance for various pressure levels is equal within a site on a subject. The p-value is a very important result of an ANOVA calculation. The p-value is a calculated probability of finding the observed results when H_0 is true. If the calculated p-value is less than the significance level then, H_0 is rejected[49]. The choice of significance level is arbitrary. Conventionally, 5%, 1% and 0.1% (p-value < 0.05, 0.01 and 0.001) are used. A p-value less than 0.05 is considered statistically significant and a p-value less than 0.001 is considered statistically highly significant[49].

ANOVA was conducted on all the data and showed that the base level absorbance was significantly different than the absorbance at any pressure level. The p value for all eight sites was less than 0.001 and on further analysis (Figure 4-6 and 4-7) showed that the base level absorbance across all subjects for all sites was significantly different than the absorbance at any pressure level.
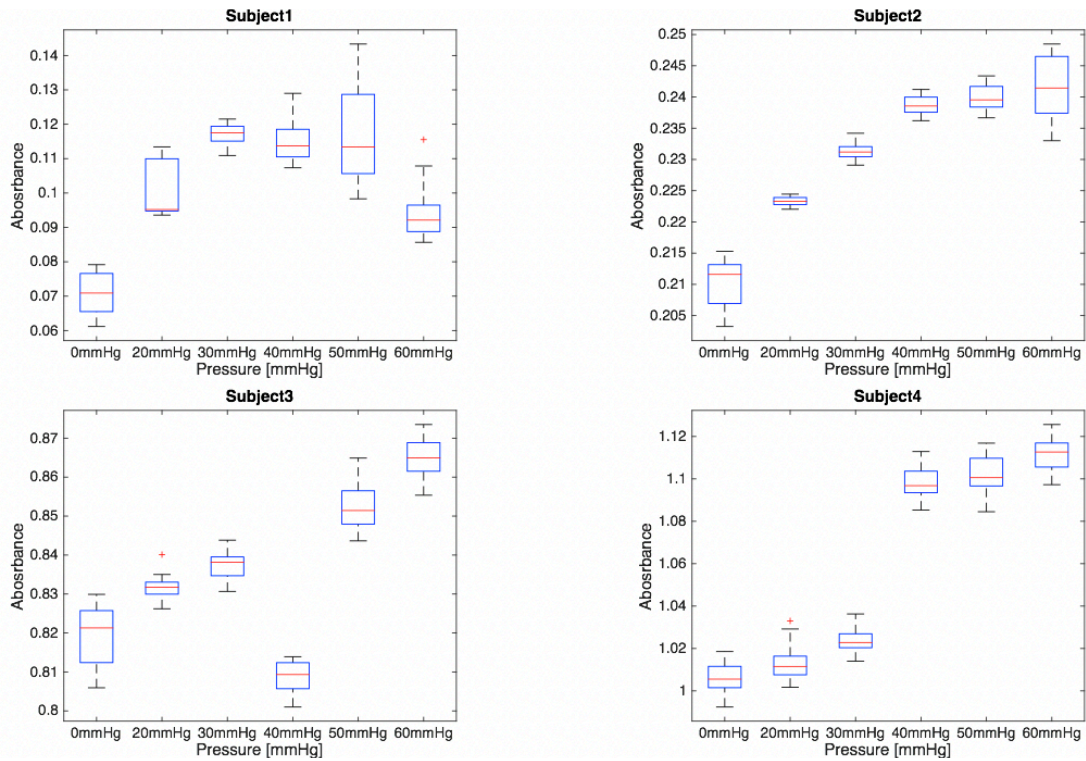
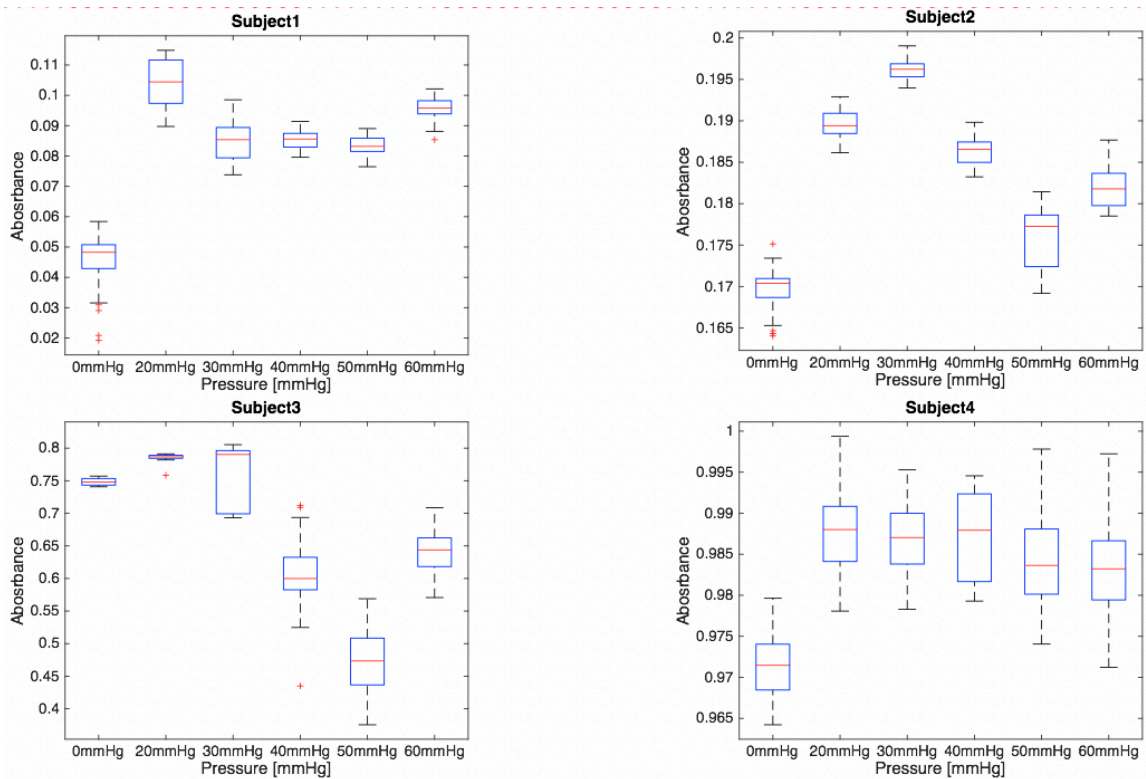*Figure 4-4: Box plots for all subjects (7 cm from elbow)*

Figure 4-5: Boxplot for all subjects (7 cms from wrist)

From Figures 4-4 and 4-5 one can see that the there is no clear trend for the effect of increasing pressure on the skin. The patterns for incremental pressure changes are not consistent across subjects. But on looking closer, the absorbance at each pressure level is always higher than absorbance at base level (0 mmHg). The inconsistencies in this data can be attributed to the fiber optic holder and the way pressure was induced on the skin, any slight movements that might have occurred during data acquisition and not having enough stability to rest the arm during the entire period of data collection.

Figure 4-6 and 4-7 show the results of the post-hoc analysis of the data. The analysis was conducted using the multcompare function on MATLAB. The results were shown as an interactive plot and the base level was chosen to test if all the other pressure levels were significantly different from the base level. Every pressure level highlighted in red implies that the mean absorbance at that pressure level is significantly different from the mean absorbance at 0 mmHg (highlighted in blue).
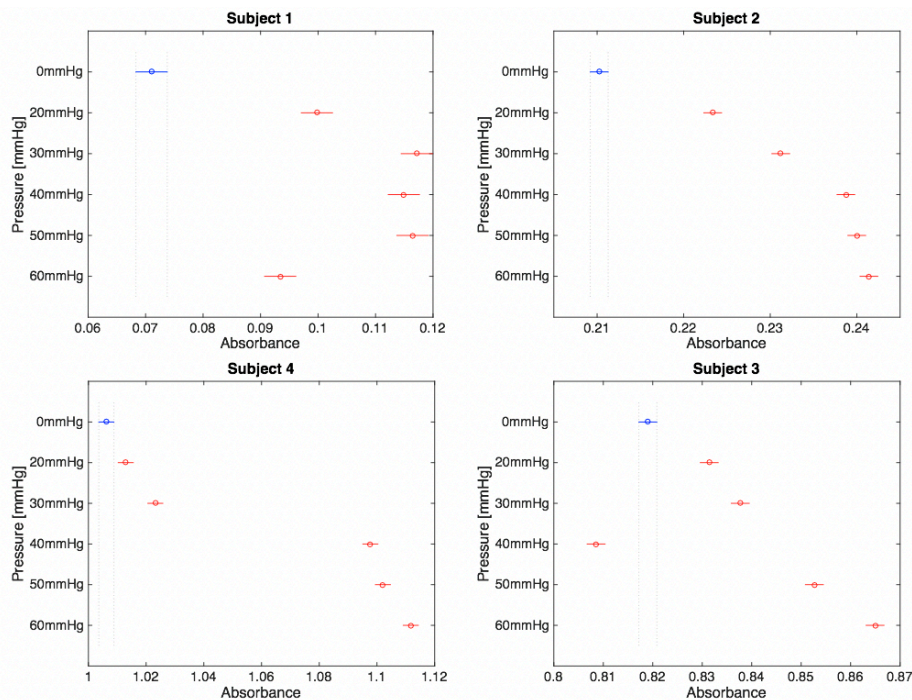

Figure 4-6: Multiple comparison test for all subjects: 7cms from the elbow
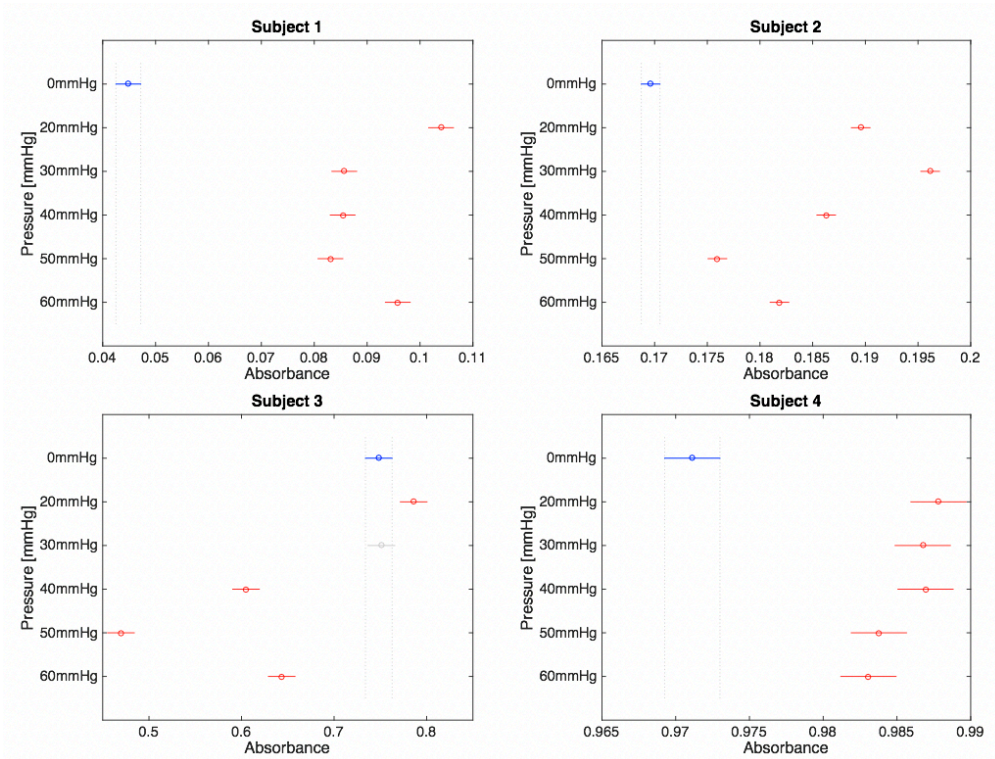
Figure 4-7: Multiple comparison test for all subjects: 7 cms from the wrist

Absorbance at 0 mmHg and 30 mmHg is compared in Figures 4-8 and 4-9 for all subjects. The absorbance at 30 mmHg is always higher than base level absorbance for all subjects at both sites.
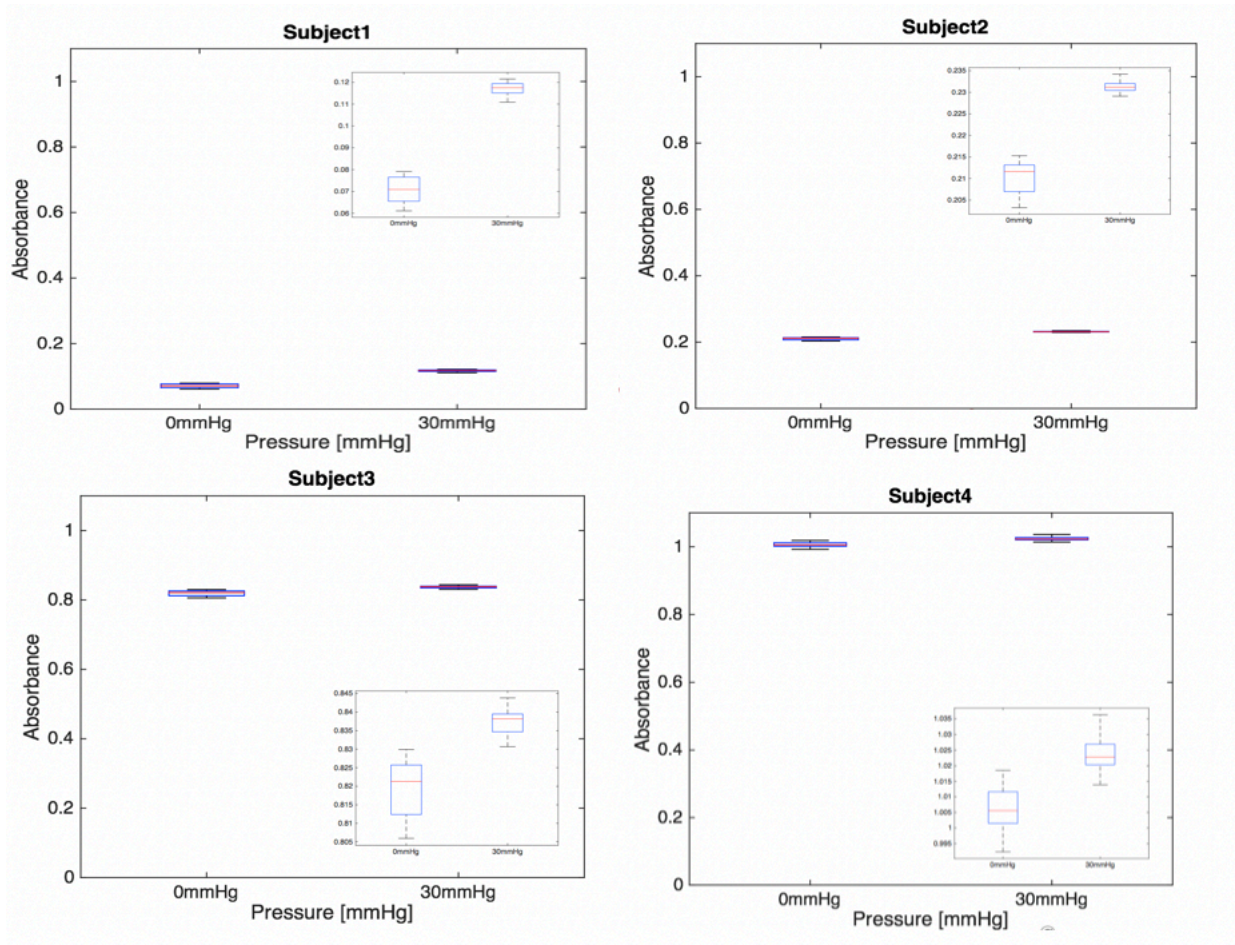
Figure 4-8: A comparison of absorbance at base level and 30 mmHg (7 cm from elbow)

Baseline absorbance is higher for dark skinned subjects (subject 3 and subject 4) because of a higher amount of melanin present in their skin. Subject 3 is highly skewed when compared to other subjects. This is attributed to the fact that the measurements at a certain pressure level had a lot of variation in them. The only reason for this happening would be due to movement during data collection.
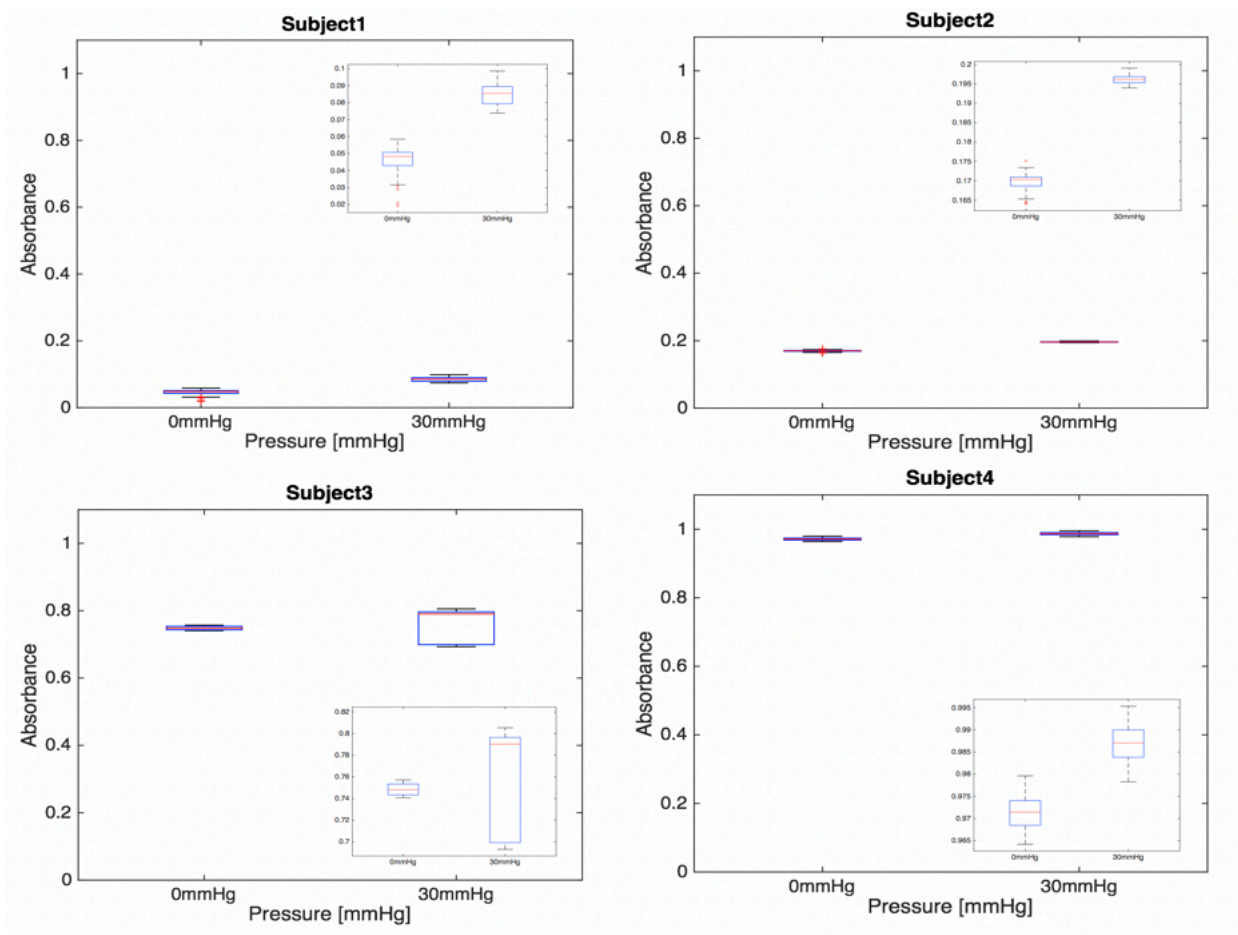
Figure 4-9: A comparison of absorbance at base level and 30 mmHg (7 cm from the wrist)

In Figures 4-8 and 4-9 above the magnitude of change in absorbance is higher for light skinned subjects (subject 1 and subject 2) than dark skinned subjects (subject 3 and subject 4). This can be due to the melanin content being higher because the melanin signals are not separated in this data processing[10]. But regardless all subjects showed an increase in absorbance at 30 mmHg when compared to baseline measurements and even though the magnitude of change of absorbance was lower in dark skinned subjects, the absorbance at 30 mmHg was still found to be significantly different from baseline absorbance.

Chapter 5 IPHONE BASED SPECTROMETER

5.1 Objective

The main objective of this research was to develop a low cost optical spectroscopy system to assess blanch response in normal skin. Smartphones, in the recent years, have gotten very advanced with their cameras. Therefore, the idea of developing a smartphone based spectrometer was introduced in this research. The main objective of this part of the research was to develop a smartphone based spectrometer which could, in the future, be converted into a 3-D mounted case to aid in early pressure ulcer diagnosis.

5.2 Transmission grating based setup

A spectrometer operates on the principle of guided light being directed to a diffraction grating and the spectra is subsequently analyzed using detector optics. Therefore, to turn a smartphone in to a spectrometer a diffraction grating was needed.

A transmission grating based set up was created as a first pass bench top design to put the above-mentioned concepts into practice. The setup was heavily inspired by the work of Smith *et al*. The setup is comprised of an iPhone 6 with a transmission grating attached on the camera. The grating used was a 1000 lines/mm grating. Light guided through a fiber optic is mounted on one end of a black collimating tube. The purpose of the tube is to guide light to the cellphone camera. A 1 mm slit was attached to one end of the tube to ensure collimation of light[35]. Figure 5-2 is an image of the first pass bench top setup constructed using a transmission grating.
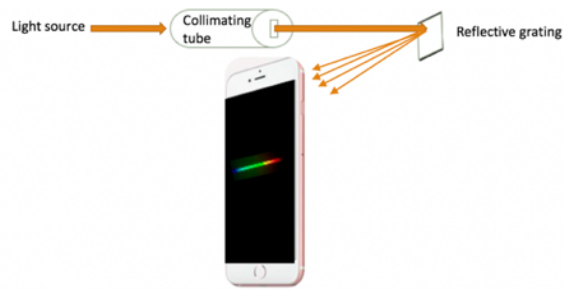
Figure 5-1: Schematic of the basic design for a smartphone based spectrometer

Figure 5-3 is the image of the spectra imaged on the iPhone. As a first pass design, the set up worked well enough where a clear spectrum was seen by the iPhone camera. This is going to be characterized in later on in this chapter.

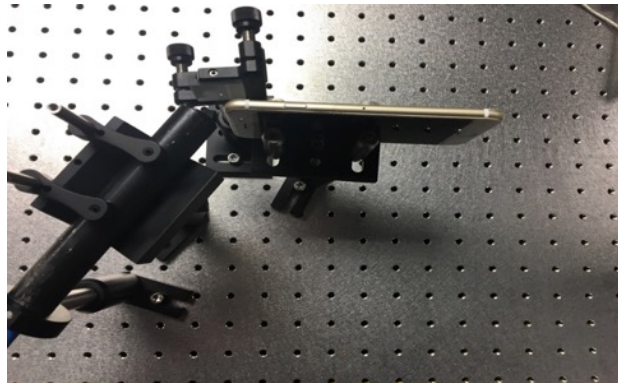*Figure 5-2: Bench top setup with a transmission grating*

Figure 5-3: Spectra of a tungsten halogen lamp as imaged on the iPhone

5.3 Reflection grating based setup

5.3.1 Reflection grating based setup type 1

A reflection grating based setup was created as an iteration to the transmission grating based setup because reflectance gratings have a better efficiency than transmission gratings. This design was also created because this bench top setup was created with a vision of making it a 3-D printed mount on the iPhone. A transmission grating based setup did not appear to be viable for a 3-D printed mount on the phone with its own light source.

Figure 5-4: Bench top setup with a reflection grating: Type 1

Figure 5-5: Spectra of a tungsten halogen lamp as imaged on the iPhone (reflection grating setup)

5.3.2 Reflection grating based setup type 2

The images taken with the previous two setups showed a lot of black space. To utilize this blank space, a second iteration of the reflection grating based setup was constructed. This setup was different from the previous reflection grating based setup in two ways. The collimation tubes were 3-D printed to allow for better collimation of light and to prevent light from escaping from the sides of the slit. A second tube was attached to the camera of the phone as seen in Figure 5-6.

Figure 5-6: Reflection grating based setup type 2

This was done to cut off the camera's field of view so that no stray light was being captured in the images taken and to increase the dimensions of the images captured. A big difference between this setup and others was the selection of ISO and Exposure time on the camera. ISO is the sensitivity of the camera sensor to light. A higher ISO implies that the sensor will be very sensitive to light and is often used in low light situations. Exposure time is the amount of time a camera sensor is exposed to light before an image is taken. In other words, a higher exposure time allows for more light to hit the camera sensor. For this setup the ISO and exposure time were set to a maximum to see whether there was any extra light hitting the camera sensor that could be giving inaccuracies during the image processing.

Figure 5-7 shows the spectrum from a tungsten halogen lamp captured used the type 2 bench top setup.
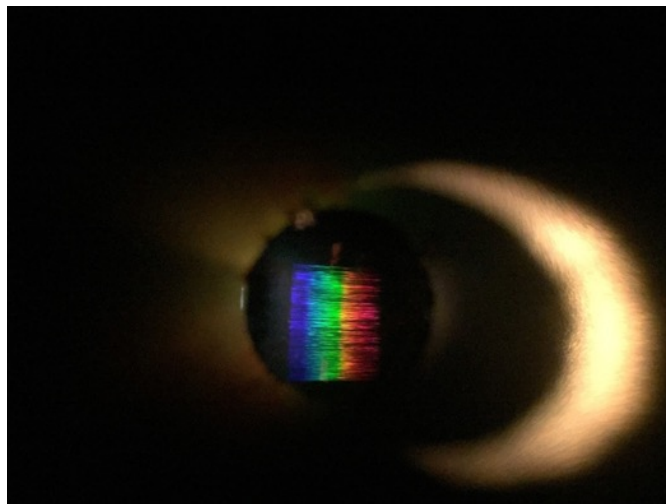
Figure 5-7: Tungsten halogen lamp spectra obtained from reflection grating setup type 2

From Figure 5-7 it is quite evident that there is an entire rectangular region of spectra that is now visible and being imaged instead of the horizontal thin line of a spectrum that was visible in Figure 5-5. The analysis and characterization of these spectra further into this chapter will better explain why this was done.

5.4 Characterization of an iPhone based spectrometer

5.4.1 Wavelength calibration

The algorithm described below has been used before to characterize smartphone spectrometers [35-37]. The purpose of this process is to relate the pixel location on an image to a certain wavelength. For this, characterized light sources of a single wavelength were chosen and imaged with the bench top setups mentioned above. By using single wavelength light sources, it is possible to see that the pixel location of the imaged spectrum changes linearly according increasing wavelength. This can be seen from the grating equation because each wavelength of light is diffracted at a different angle and the location of the pixels imaged according to these angles is linearly related to the wavelength [36,37].

For this analysis two different light sources were used. For the transmission grating setup, a monochromator coupled with a tungsten halogen light source was used to manually select different wavelengths of light and image them. Meanwhile, the reflection grating setups used an LED light source with LEDs of 470 nm, 502 nm and 590 nm.

5.4.1.1 Transmission grating based setup

For the transmission grating based setup, 13 different wavelengths ranging from 440 nm to 700 nm in 20 nm increments were imaged. Figures 5-8 show some of the images obtained using a monochromator.

Figure 5-8: 440 nm, 580 nm and 700 nm as imaged on the iPhone

The monochromator images were analyzed on MATLAB individually and intensity versus pixel index plots were created for each image. Figures 5-9, 5-10 and 5-11 are plots of intensity vs pixel index for wavelengths of 440 nm, 580 nm and 700 nm respectively.

Figure 5-9: Intensity vs Pixel index for 440 nm
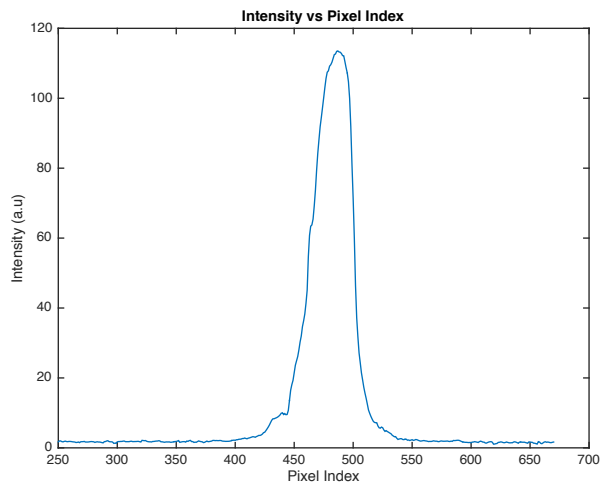
Figure 5-10: Intensity vs Pixel index for 580 nm

34
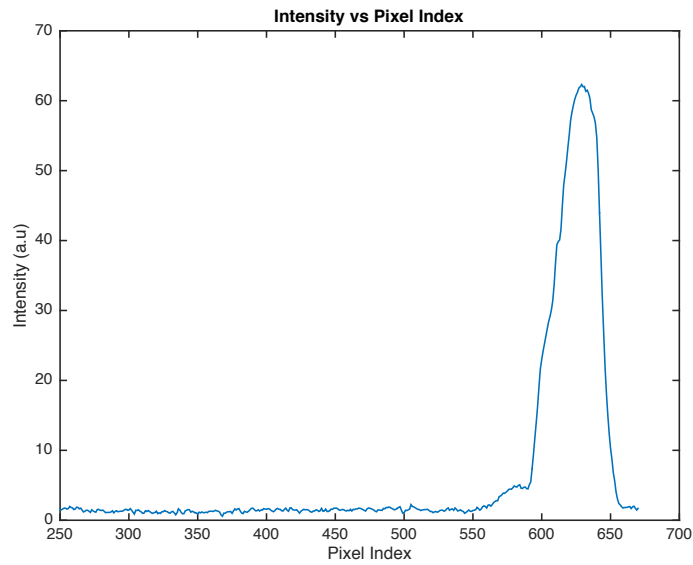
Figure 5-11: Intensity vs Pixel index for 700 nm

From the line plots in Figures 5-10, 5-11 and 5-12, one can clearly see a shift in the intensity peaks from left to right. Thirteen such plots were obtained from the 13 images taken at different wavelengths and a median pixel index was calculated from each plot. The median pixel location from each of these distributions was then plotted against wavelength (Figure 5-13).
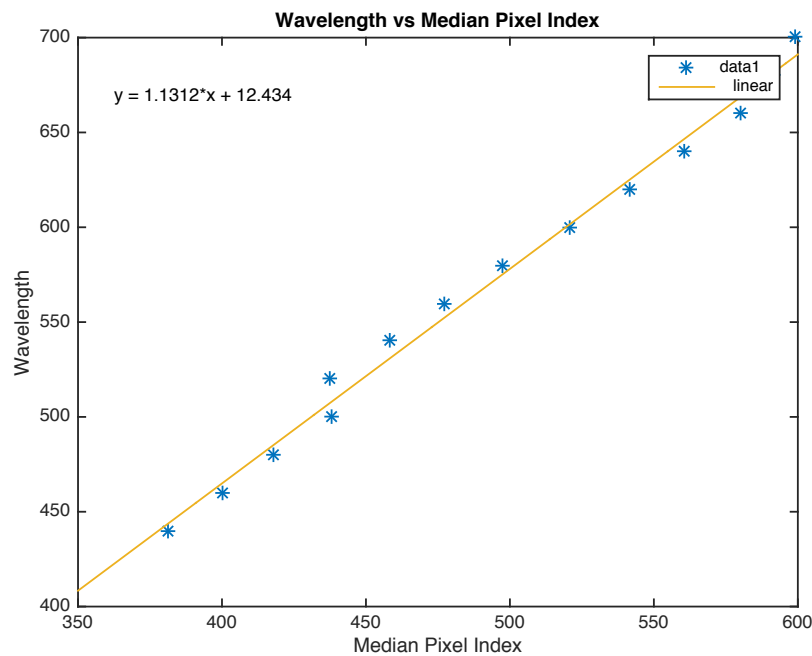
Figure 5-12: Wavelength vs Median pixel index for transmission grating setup

Figure 5-13 has an evident linear fit. The wavelength calibration equation was then found by fitting a linear regression through the points. The wavelength calibration equation is shown below.

This allows for the images to now be characterized using wavelength and intensity. The algorithm stayed the same for the reflection based setups. But the results will be discussed below.

5.4.1.2 Reflection grating based setup type 1

For this setup, an LED light source with 470 nm, 502 nm and 590 nm LEDs was employed. This was done because even though the monochromator was a reliable way of obtaining characterized spectra at any specific wavelength in the visible range, it does have a certain amount of noise that can attribute to not obtaining an accurate median pixel location. The images obtained from the LED light source are shown below (Figure 5-13).

Figure 5-13: 470, 502 and 590 nm spectra from Stellarnet SL1 LED lamp

The line plots for these spectra are shown in Figures 5-15, 5-16 and 5-17.

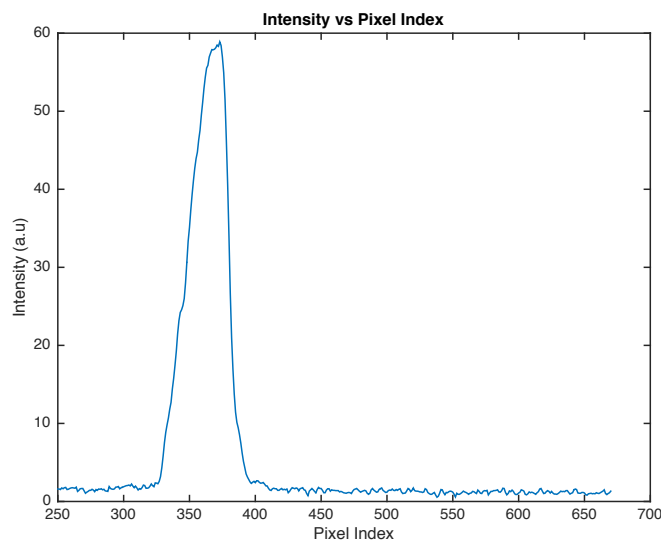*Figure 5-14: Intensity vs Pixel index at 470 nm*
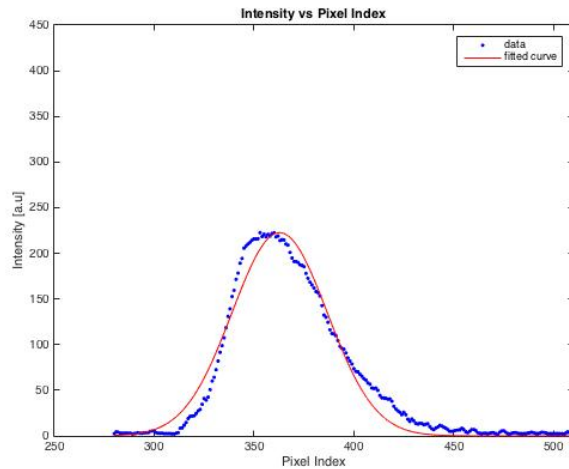
Figure 5-15: Intensity vs Pixel indx at 502 nm
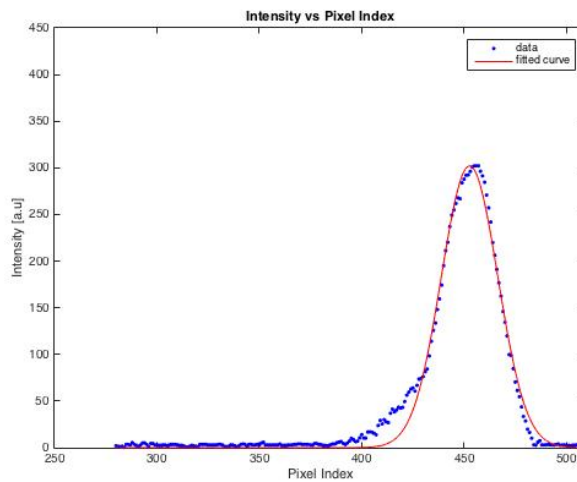
Figure 5-16: Intensity vs Pixel index at 590 nm

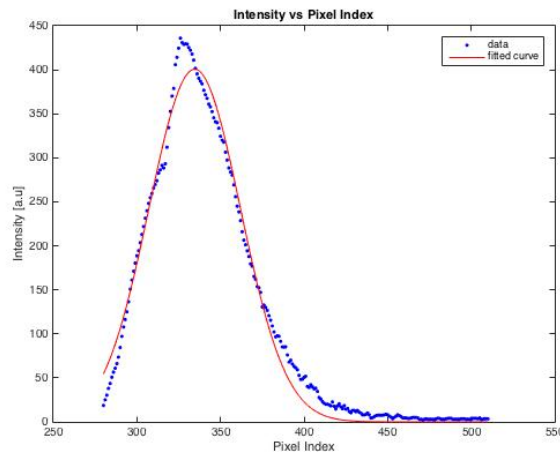A one term Gaussian curve was fitted to these line plots and the peak of the Gaussian fit was used as the median pixel index for wavelength calibration. This was done to ensure that none of the noise in the line plots was affecting the median pixel index calculation.
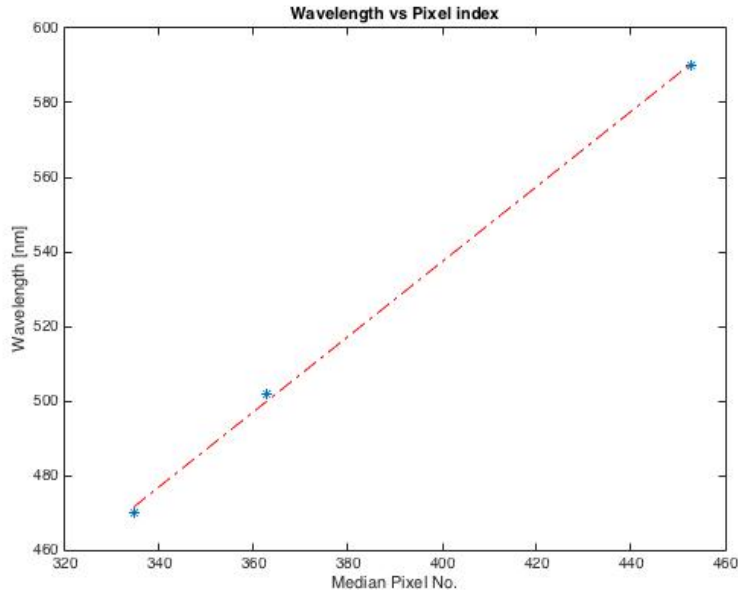
Figure 5-17: Wavelength calibration for reflection grating setup type 1

5.4.1.3 Reflection grating based setup type 2

This setup was slightly different from the previous one. The two changes made to this setup were the 3-D printed collimating tube was used instead of a collimating tube with a slit attached on it. This was done to ensure no extra light was escaping from the spaces between the tube and the slit attachment. Secondly, a collimating tube was attached to the camera of the phone to ensure that the camera's field of view was limited so that the camera would focus only on the spectra and not on anything else. The image processing and wavelength calibration algorithm for this setup was the same as the previous setup discussed in Chapter 5.3.1.2.

Figure 5-19 represents the wavelength calibration plot for the reflection grating based setup type 2.
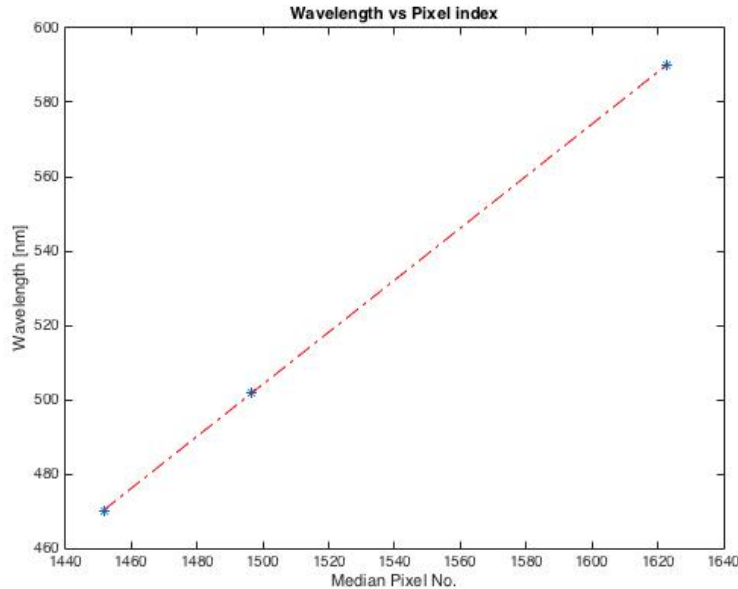
Figure 5-18: Wavelength calibration for reflection grating based setup type 2

A linear egression fit was conducted on MATLAB to extract the relationship between pixel index and wavelength.

5.4.2 Intensity calibration

Now that all the setups were calibrated for wavelength, it was possible to obtain plots of intensity vs wavelength just as a spectrometer would. However, there was still a need to check whether these plots would match the results of an actual spectrometer. Previous work already shows that a phone based spectrometer is always in need for an intensity calibration[35-37]. This section outlines the process of intensity calibration and discusses the results obtained from each setup.

An intensity calibration starts with the calculation of a correction factor. A known standard light source (in this case Tungsten Halogen) is imaged through the iPhone spectrometer and the results are analyzed on MATLAB using the algorithm discussed thus far. The theoretical spectra of the light source (i.e. the spectra obtained from any standard spectrometer, for this research Ocean Optics 4000 USB was used) is then compared to the spectra obtained from the iPhone. A correction factors is calculated by comparing these two spectra. The correction factor is calculated using a reference light source. A reference light source in this research is simply a light source used to calculate the correction factor. To test the intensity calibration, the correction factor is then applied to a different light source which is referred to as the target light source. In

39

theory, the correction factor should be able to produce a curve very similar to the actual spectra of the target light source.

5.4.2.1 Transmission grating based setup

Figure 5-20 is the uncorrected spectra of a tungsten halogen lamp, obtained after the wavelength calibration. The actual or theoretical spectra of the lamp was obtained from Ocean Optics USB 4000 spectrometer along with the use of Spectrasuite. Figure 5-21 is the theoretical/actual spectra of a tungsten halogen lamp as obtained from the spectrometer.
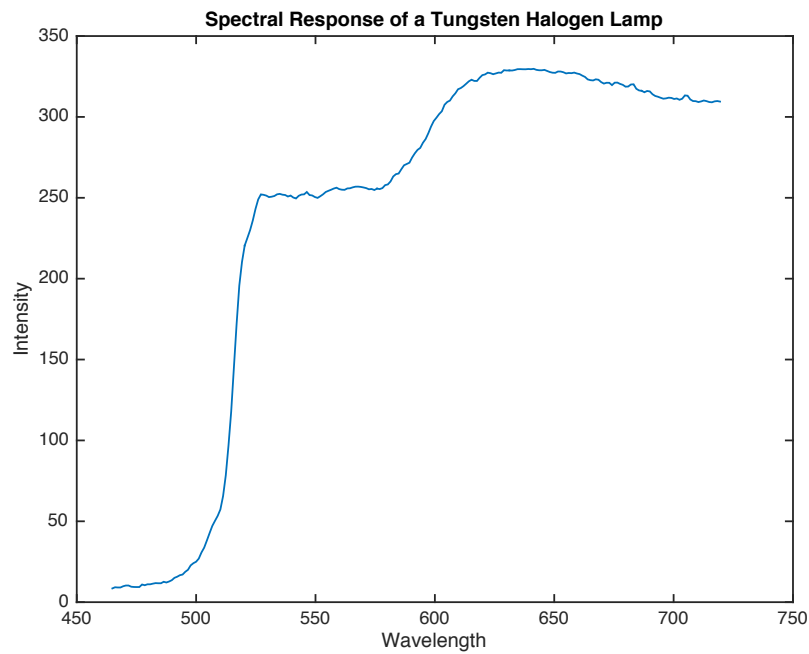
Figure 5-19: Uncorrected iPhone spectra of a tungsten halogen lamp (transmission grating based setup)
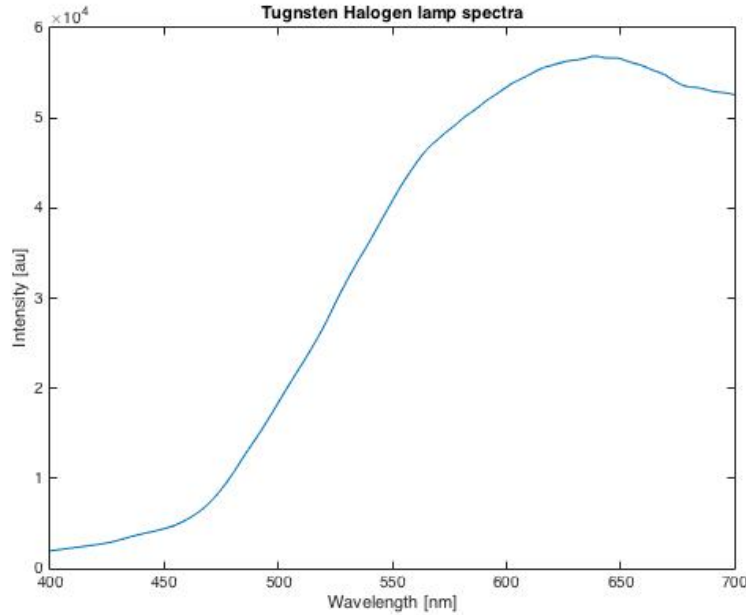
Figure 5-20: Actual spectral response of a tungsten halogen lamp

When looking at Figures 5-20 and 5-21, the shapes differ significantly. Therefore, a correction factor is needed. For the first pass setup with a transmission grating the correction factor was calculated by simply dividing the measured spectrum by the actual spectrum. The correction factor formula is given below.

$$C(\lambda) = \frac{I_m(\lambda)}{I_{acutal}(\lambda)} \tag{2}$$

Where C(λ) represents the correction factor. $I_m(\lambda)$ is the measured spectrum of the tungsten halogen lamp as obtained from the iPhone based setup. $I_{actual}(\lambda)$ is the actual spectrum of the tungsten halogen lamp as obtained from the spectrometer. This correction factor was calculated from the tungsten halogen spectra and was re applied to the uncorrected tungsten halogen lamp spectra in Figure 5-19. Essentially, the correction factor is calculated using the spectra of a known light source and then applied to a completely different light source to see how effective it is. the "forced fit" of the tungsten halogen spectra is shown in Figure 5-22.
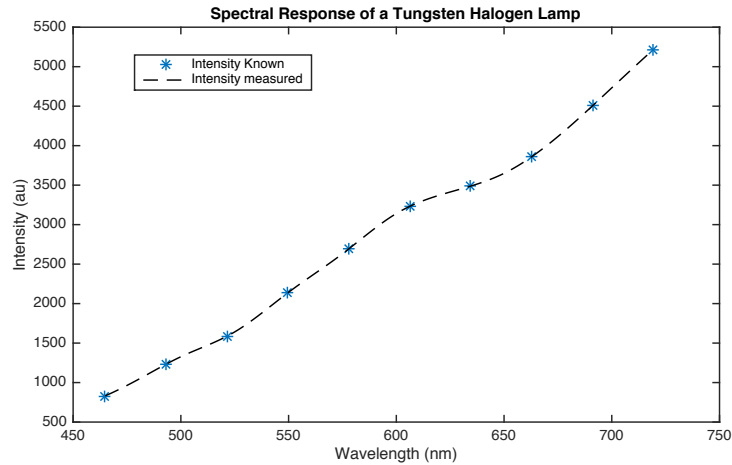
Figure 5-21: Corrected spectra of a tungsten halogen lamp (transmission grating based setup)

After this stage, the transmission grating based setup was changed to a reflection grating based setup simply because reflection gratings are more efficient and a reflection grating based setup made more sense if the bench top setup had to transform into 3-D printable mount. Due to time constraints and to make decent progress in this research, no target source was used to test the transmission grating based setup since it was a first pass setup to test certain concepts.

5.4.2.2 Reflection grating based setup type 1

The tungsten halogen lamp was used a reference light source for the correction factor calculation. The measured spectra from a tungsten halogen lamp is shown in Figure 5-23.
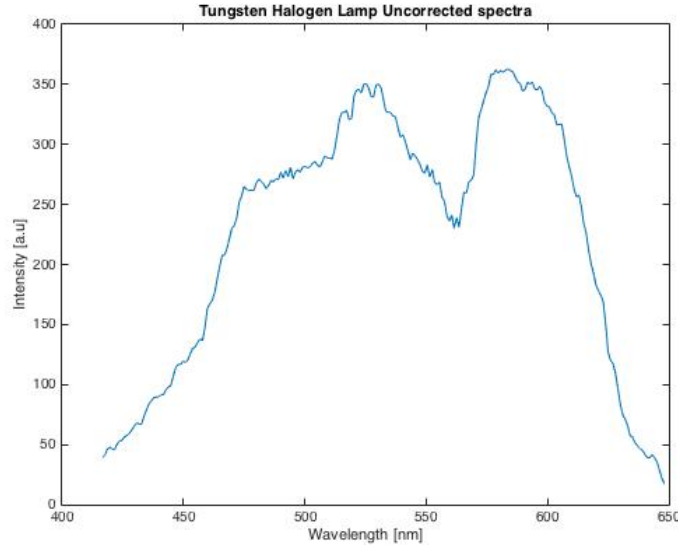
Figure 5-22: Uncorrected spectra of a tungsten halogen lamp (Reflection grating based setup type 1)

The calculation of the correction factor was different with this setup. Numerous amounts of calibration runs have been conducted using this setup and the results were not good. The corrected and actual spectra did not look comparable at all. For this reason, two changes were made. Firstly, it can be seen from Figure 5-21 that the actual spectrum of a tungsten halogen lamp has a much different intensity scale than the uncorrected (measured) spectrum. This is why the actual spectrum of the lamp was normalized by dividing the entire intensity spectrum by the maximum intensity. This was done to ensure that when the correction factor is applied to the target source, it does not get a shape that is heavily influenced by the actual spectrum of the reference source. Secondly, the correction factor formula was changed such that each color channel had its own correction factor[37]. This is going to ensure that each color channel gets corrected individually in hopes of yielding a better result. The correction factor formula is given by the equation below.

$$R(\lambda) = r(\lambda)I(\lambda)$$
$$B(\lambda) = b(\lambda)I(\lambda)$$
$$G(\lambda) = g(\lambda)I(\lambda)$$

I(λ) is the actual spectrum of the reference light source. R(λ), B(λ) and G(λ) are the measured color channels of the reference light source. $r(\lambda), b(\lambda)$ and $g(\lambda)$ are the individual channel response functions or correction factors. The uncorrected spectrum can then be converted into a calibrated spectrum by a least squares formula shown below[37].

43

$$I'(\lambda) = \frac{r(\lambda)R'(\lambda)+b(\lambda)B'(\lambda)+g(\lambda)G'(\lambda)}{r^2(\lambda)+b^2(\lambda)+g^2(\lambda)}$$

Where $I'(\lambda)$ is the corrected spectrum of the target source. $R'(\lambda)$, $B'(\lambda)$ and $G'(\lambda)$ are the measured color channels of the target source. The response functions or the correction factors are calculated from the reference source as mentioned above.

This correction factor algorithm was applied to a LED light source. The tungsten halogen lamp was treated as the reference source and white LED was treated as the target source. Figure 5-24 shows the uncorrected target light source spectrum.
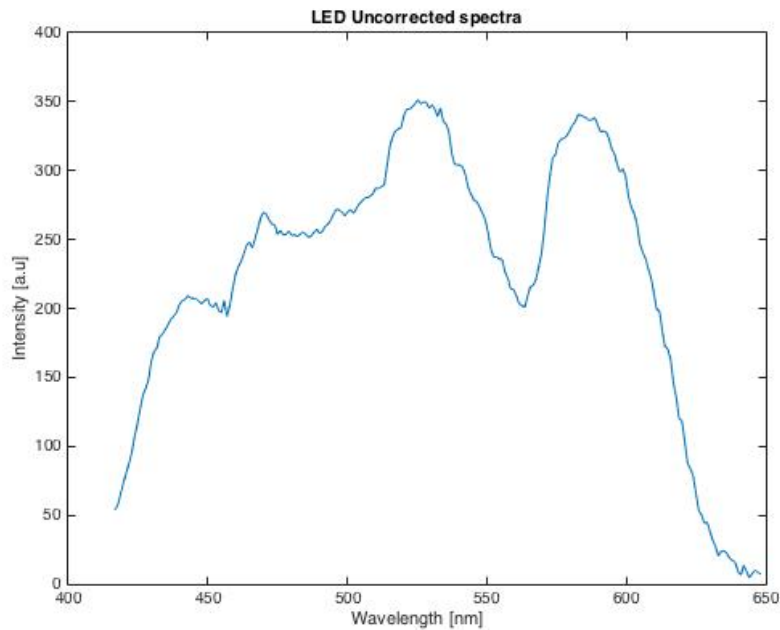
Figure 5-23: Uncorrected spectra for a white LED light source (Reflection grating setup type 1)

The correction factor algorithm was computed in MATLAB and Figure 5-25 shows the comparison between the actual LED spectrum and the corrected LED spectrum.

44
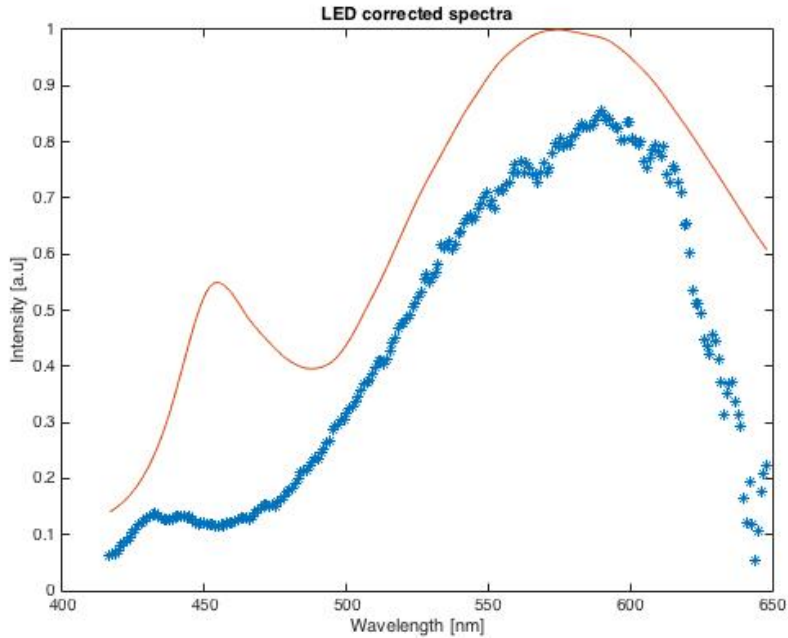
Figure 5-24: Corrected spectra for white LED light source (Reflection grating setup type 1)

The orange curve in Figure 5-25 is the actual spectrum of the light source and the blue curve is the corrected spectrum. The intensity calibration is carried out to get a match of the shape, and not necessarily the exact values. This is because, the values are bound to be off by some scale because the iPhone images are being processed on MATLAB while the actual spectrum is being processed on Spectrasuite. The shape is not entirely good enough to call it a successful intensity calibration but it would be considered an overall good match for the characteristic shape of a white LED spectrum. A missing key feature, however, is the characteristic peak of the white LED spectrum at approximately 450 nm. Therefore, this fit was not considered successful.

The intensity calibrations were also conducted in the opposite direction whereby the white LED was used as a reference source and the tungsten halogen was used as the target source. Figures 5-26 shows the corrected tungsten halogen spectrum in comparison with the actual spectrum, when the correction factors are obtained using white LED light source as a reference light source.

45
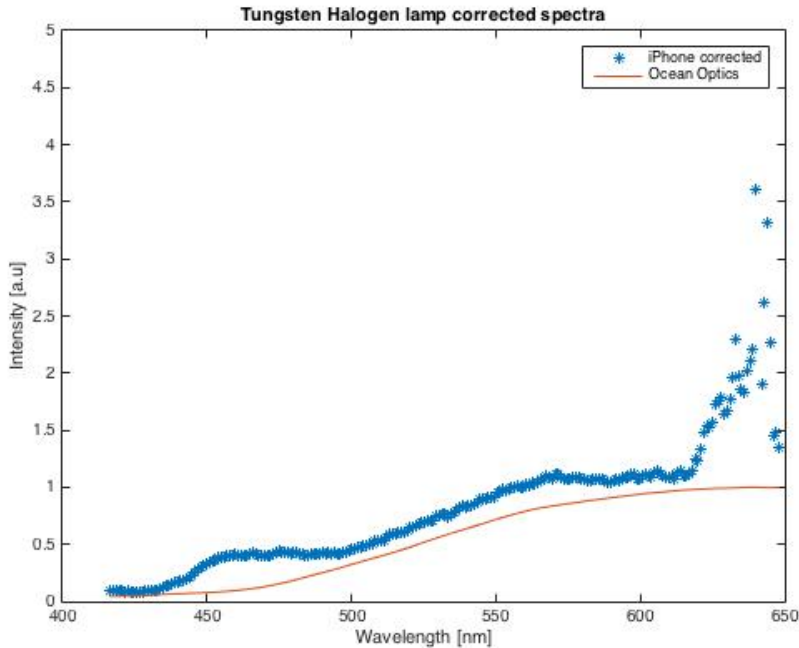
Figure 5-25: Corrected spectra of tungsten halogen light source (Reflection grating setup type 1)

From Figure 5-25 it is quite clear that the shape is not a good match to the actual spectra. This is because one can almost see an imprint of the characteristic LED spectrum shape on the corrected tungsten halogen curve in blue. This imprinting was mentioned earlier in this chapter when the actual spectra of the reference sources were normalized. One can also see that the corrected spectrum has a lot of random noise after 600 nm. All the key observations will be discussed and explained at the end of this chapter when all setups will be compared.

5.4.2.3 Reflection grating based setup type 2

The entire algorithm for this setup remained the same as the one in Chapter 5.5.2.2 and therefore will not be repeated. Figure 5-27 shows the corrected white LED spectrum for this setup. From the plot it can be seen that the shape of the corrected cure is no match to the actual spectrum, moreover it shows that the shape is highly influenced by the actual shape of the reference spectrum and shows chaotic behavior after 600 nm.

Figure 5-26: Corrected spectra for white LED light source (Reflection grating setup type 2)

Figure 5-27 represents the corrected spectrum for a tungsten halogen light source whereby the white LED was used as a reference source to calculate the correction factors.
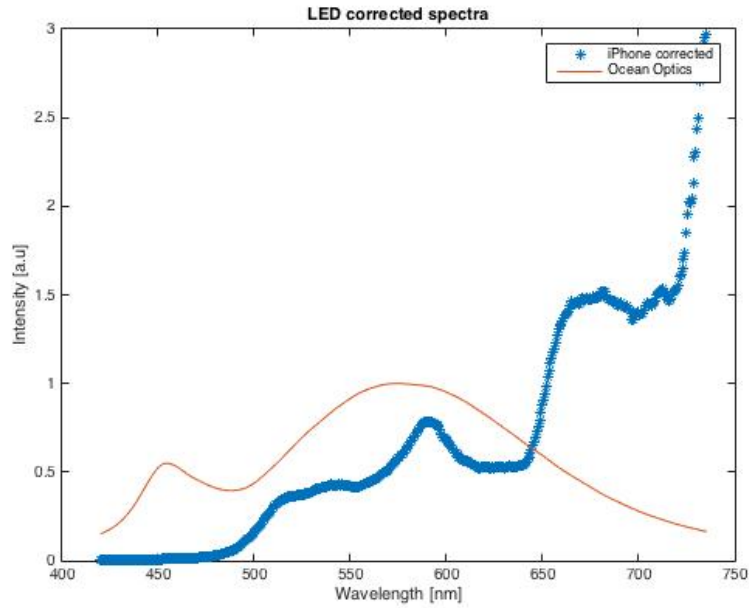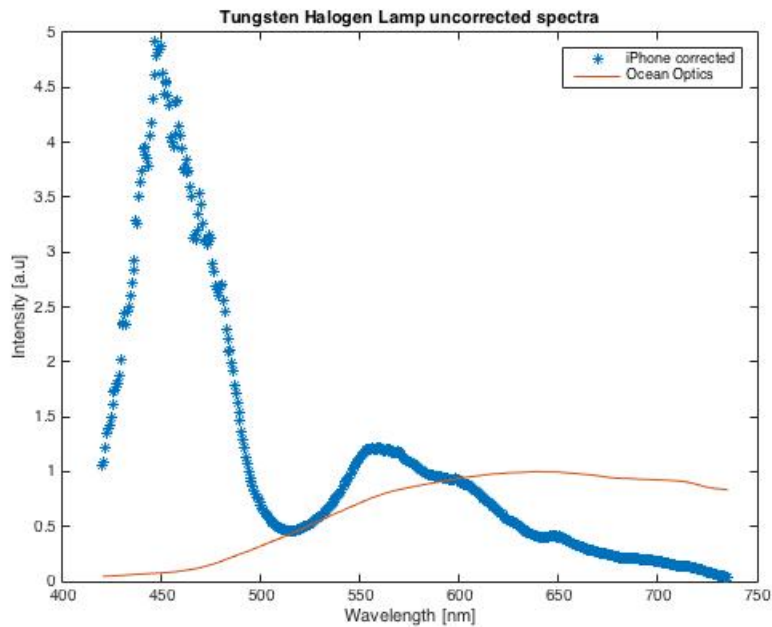

Figure 5-27: Corrected spectra for tungsten halogen light source (Reflection grating based setup type 2)

Figure 5-27 shows that the corrected spectrum shape highly mimics the characteristic shape of the white LED spectrum. Its due to these repeated unknown inconsistencies in all the setups that the research had to be moved forward without being able to successfully 3-D print a mountable spectrometer on the iPhone.

A comparison between all three setups and their drawbacks are discussed below. The transmission grating based setup was simply used as a first pass setup and a proof of concept for this research. Even though the results looked promising, this setup was not stable enough to carry out repeatable experiments and would not be a practical bench top model to depict the pathway of optics in the 3-D printable mount. A reflection grating based setup was created to optimize the image quality since reflection gratings are said to be more efficient than transmission gratings. Both reflection grating based setups had optical pathways that could be translated into a 3-D printable mount in the future.

Type 1 setup with reflection grating came the closest to mimicking the actual spectra. The drawbacks with this setup were the fact that there was stray light coming on to the grating and creating noise. The shapes, however, were a close match for the actual shapes of the spectra. There was a slight imprint from the reference light source spectra but it was considerably less than what was seen in the Type 2 setup. The noise in Figures 5-25 and 5-26 can be attributed to the Bayer filter and the IR sensor of the iPhone camera. The filter and the IR sensor of the iPhone camera caused the light after approximately 620 nm to be slowly cut off and this could be the reason for the inaccuracies observed in those regions[35]. These inaccuracies were also noticed in Figure 5-27 and 5-28 where the intensity either went to zero where it wasn't supposed to (Figure 5-28) or it skyrocketed for no apparent reason (Figure 5-27).

Type 2 setup with reflection grating was constructed with the intentions of improving on the type 1setup. The 3-D printed collimating tube and a collimating tube attached to the camera were there to ensure no stray light was getting on the grating or the camera sensors. Despite this, Figures 5-27 and 5-28 show worst results than the previous setup. Camera controlling parameters such as ISO and Exposure time were maximized so that the images could show any stray light or inconsistencies. Maximizing the ISO and exposure time did show that the camera had been

looking at only a part of the bigger spectrum. The spectra shown in Figures 4-5 and 4-7 show that the latter occupies a much bigger area. This was one of the only positives of this setup. However, maximizing the ISO and exposure time could have also created more harm by making the camera sensor extremely sensitive to any stray light and this might be one of the reasons for Figures 5-27 and 5-28 looking as terrible as they do.

Overall, there have been general comments about the difficulty of calibrating an iPhone based spectrometer and here are few reasons why. Measurement and calibration consistency of an iPhone based spectrometer are very hard to achieve because it requires the control of white balance and focus. While there are apps that allow the user to control these factors, the resulting images are also highly processed and may not be accurate for spectral calibration. iPhones are known for their sensors and high amounts of post processing. This could be a reason for not being able to see key deductions from analyzing these images. There are certain key features of an image that are lost after such processing. iPhones also do not give a user enough access to where the raw data of an image can be accessed. For this reason, it will be better to further this research using an android where the user is given control of the camera parameters and raw form of an image is accessible[37].

Chapter 6 SUMMARY AND RECOMMENDATIONS

6.1 A portable reflectance spectroscopy system for measuring blanch response in normal skin

The spectroscopy system did not work as expected, in fact the fiber optic holder along with the weights induced blanching on the areas around the edge of the disk which caused blood to be pushed towards the center of the disk. The incremental pressure changes were implemented in this study in an effort to characterize the response of tissue under increasing pressure. But due to the experimental setup failing and inconsistencies during data collection, a proper trend or pattern could not be found to characterize the effect of incremental pressure changes across all subjects.

The study was still successful in proving that the effect of pressure on skin can be observed using DRS. ANOVA within subjects showed that the baseline absorbance was significantly different than the absorbance at any pressure level. All p values across subjects within all testing sites were found to be less than 0.001. The difference between baseline absorbance and 30 mmHg of pressure was looked at closely. Across all subjects, the absorbance at 30 mmHg was found to be higher than baseline absorbance. The magnitude of absorbance change for dark skinned subjects was significantly lower than that for light skinned subjects. This was attributed to the fact that the contribution of melanin could not be ruled out of the data analysis algorithm.

This study did not quite prove what it was set out to do but nonetheless it did prove that skin changes with pressure application can be detected spectroscopically. The diameter of the disk was much bigger than the diameter of the reflectance probe, this led to an uneven distribution of pressure while using weights to induce pressure on to the forearm. A design with a much smaller disk will be much better for inducing pressure that acts evenly on the entire disk and simulates blanching in the sensing volume of the probe. The idea of using weights to simulate pressure is a good first pass design, but a spring-loaded fiber optic holder could work better in this case and has been used in a study before to successfully simulate a blanch response[10].

6.2 iPhone based spectrometer

The iPhone based spectrometer was developed as an alternative to introduce a low-cost device that could mimic everything a portable reflectance spectroscopy setup is capable of doing. Various iterations of the bench top design were performed in an effort to successfully calibrate the phone based spectrometer.

The reflection grating based setups produced the most promising results but even after calibration, these spectra did not come very close to the actual spectra. During these designs, various factors that affect proper image acquisition, came to light. Factors like the camera sensor and filters played a big role in acquiring a calibrated spectrum. Studies have also mentioned the importance of controlling the white balance and focus on the camera to acquire a spectrum that can be successfully calibrated[37]. iPhones also highly process the images that are taken on their cameras and do not let the user have any access to the raw images. For this reason, android was suggested by Zhang *et al.* because of the possibility of being able to access the images in their raw form.

Further recommendations for this concept would involve replacing the iPhone with an android. Controlling various camera parameters such as ISO, exposure, white balance and focus would shed light on better intensity calibration. The raw images should be accessed, and the phone based spectrometer should be characterized using those images. The benchtop setup needs to be optimized so that there is absolutely no movement of the phone during image acquisition. A millimeter of movement would shift the pixels by large magnitude.

Chapter 7 REFERENCES

1.   Unit AM, Works C, Management A, Health Q. Pressure Ulcer. www.nlm.nih.gov/cgi/mesh/2009/MB_cgi?mode=&term=Pressure+Ulce r&field=entry.
2.   Anders J, Heinemann A, Leffmann C, Leutenegger M, Pröfener F, von Renteln-Kruse W. Decubitus ulcers: pathophysiology and primary prevention. *Dtsch Arztebl Int*. 2010;107(21):371-381; quiz 382. doi:10.3238/arztebl.2010.0371.
3.   World Health Organisation. ICD-10 Version:2010. World Health Organisation. http://apps.who.int/classifications/icd10/browse/2010/en. Published 2010.
4.   EPUAP-NPUAP-PPPIA International Pressure Ulcer Guidelines | EPUAP. http://www.epuap.org/guidelines/.
5.   Pressure Ulcer Category/Staging Illustrations. http://www.npuap.org/resources/educational-and-clinical-resources/pressure-ulcer-categorystaging-illustrations/.
6.   Kottner J, Balzer K, Dassen T, Heinze S. Pressure ulcers: a critical review of definitions and classifications. *Ostomy Wound Manage*. 2009;55(9):22-29.
7.   Cui F-F, Pan Y-Y, Xie H-H, et al. Pressure Combined with Ischemia/Reperfusion Injury Induces Deep Tissue Injury via Endoplasmic Reticulum Stress in a Rat Pressure Ulcer Model. *Int J Mol Sci*. 2016;17(3):284. doi:10.3390/ijms17030284.
8.   Baharestani M, Black J, Carville K, et al. Pressure , Shear , Friction and Microclimate in Context: a Consensus Document. *Wounds Int*. 2010:1-28. http://www.woundsinternational.com/media/issues/300/files/content_8925.pdf.
9.   Mayo Clinic. Bedsores (Pressure sores) Tests and diagnosis - Mayo Clinic. http://www.mayoclinic.org/diseases-conditions/bedsores/basics/tests-diagnosis/con-20030848. Published 2014. Accessed May 23, 2016.
10.   Zanca JM. Exploring methods to improve pressure ulcer detection: Spectroscopic assessment of the blanch response. 2006. doi:10.1017/CBO9781107415324.004.
11.   Wang Q, Kong L, Sprigle S, Hayward V. Portable gage for pressure ulcer detection. *Annu Int Conf IEEE Eng Med Biol - Proc*. 2006:5997-6000. doi:10.1109/IEMBS.2006.260070.
12.   Yang Y, Wang J. A design of bioimpedance spectrometer for early detection of pressure ulcer. *Conf Proc . Annu Int Conf IEEE Eng Med Biol Soc IEEE Eng Med Biol Soc Annu Conf*. 2005;6:6602-6604. doi:10.1109/IEMBS.2005.1616014.
13.   Bates-jensen BM, Mccreath HE, Pongquan V, Apeles NCR. Subepidermal moisture differentiates erythema and stage I pressure ulcers in nursing home residents. 2007:189-197. doi:10.1111/j.1524-475X.2008.00359.x.
14.   Clendenin M, Jaradeh K, Shamirian A, Rhodes SL. Inter-operator and inter-device agreement and reliability of the SEM Scanner. *J Tissue Viability*. 2015;24(1):17-23. doi:10.1016/j.jtv.2015.01.003.
15.   Swisher SL, Lin MC, Liao A, et al. Impedance sensing device enables early detection of pressure ulcers in vivo. *Nat Commun*. 2015;6:1-10. doi:10.1038/ncomms7575.
16.   Stranc MF, Sowa MG, Abdulrauf B, Mantsch HH. Assessment of tissue viability using near-infrared spectroscopy. *Br J Plast Surg*. 1998;51(3):210-217. doi:10.1054/bjps.1997.0088.
17.   Anand S, Sujatha N, Narayanamurthy VB, Seshadri V, Poddar R. Diffuse reflectance spectroscopy for monitoring diabetic foot ulcer - A pilot study. *Opt Lasers Eng*. 2014;53:1-5. doi:10.1016/j.optlaseng.2013.07.020.

18. Pike Technologies. Diffuse Reflectance – Theory and Applications.
19. Sircan-Kucuksayan A, Uyuklu M, Canpolat M. Diffuse reflectance spectroscopy for the measurement of tissue oxygen saturation. *Physiol Meas*. 2015;36(12):2461-2469. doi:10.1088/0967-3334/36/12/2461.
20. Frei RW. Diffuse Reflectance Spectroscopy ; Applications , Standards , and Calibration (With Special Reference to Chromatography). 1976;(August):551-565.
21. Zonios G, Bykowski J, Kollias N. Skin melanin, hemoglobin, and light scattering properties can be quantitatively assessed in vivo using diffuse reflectance spectroscopy. *J Invest Dermatol*. 2001;117(6):1452-1457. doi:10.1046/j.0022-202x.2001.01577.x.
22. Yu B, Shah A, Nagarajan VK, Ferris DG. Diffuse reflectance spectroscopy of epithelial tissue with a smart fiber-optic probe. *Biomed Opt Express*. 2014;5(3):675-689. doi:10.1364/BOE.5.000675.
23. Vishwanath K, Chang K, Klein D, et al. Portable, fiber-based, diffuse reflection spectroscopy (DRS) systems for estimating tissue optical properties. *Appl Spectrosc*. 2011;65(2):206-215. doi:10.1366/10-06052.
24. Nielsen KP, Zhao L, Stamnes JJ, Stamnes K. The optics of human skin : Aspects important for human health. 2008;(1):35-46.
25. Anderson RR, Parrish JA. The optics of human skin. *J Invest Dermatol*. 1981;77(1):13-19. doi:10.1016/j.artres.2008.11.002.
26. Thesis A, Hollmann J. Multi-Layer Diffusion Approximation for Photon Transport in Biological Tissue Multi-Layer Diffusion Approximation for Photon Transport in Biological Tissue. 2007;(August).
27. Jacques SL. Optical properties of biological tissues: a review; Corrigendum. *Phys Med Biol*. 2013;58(14):R37-R61, 5007-5008. doi:10.1088/0031-9155/58/14/5007.
28. Wilson RH, Mycek M. Models of light propagation in human tissue applied to cancer diagnostics. *Technol Cancer Res Treat*. 2011;10(2):121-134. doi:10.7785/tcrt.2012.500187.
29. Palmer GM, Ramanujam N. Monte Carlo-based inverse model for calculating tissue optical properties. Part I: Theory and validation on synthetic phantoms. *Appl Opt*. 2006;45(5):1062-1071. doi:10.1364/AO.45.001062.
30. Georgakoudi I, Jacobson BC, Van Dam J, et al. Fluorescence, reflectance, and light-scattering spectroscopy for evaluating dysplasia in patients with Barrett's esophagus. *Gastroenterology*. 2001;120(7):1620-1629. doi:10.1053/gast.2001.24842.
31. Ghosh, N., Mohanty, S. K., Majumder, S. K., Gupta PK. Measure- ment of optical transport properties of normal and malignant human breast tissue. *Appl Opt*. 2001;40(9):176-184.
32. Yu B, Fu HL, Ramanujam N. Instrument independent diffuse reflectance spectroscopy. 2011;16(January):1-12. doi:10.1117/1.3524303.
33. Langhout GC, Spliethoff JW, Schmitz SJ, et al. Differentiation of healthy and malignant tissue in colon cancer patients using optical spectroscopy: A tool for image-guided surgery. *Lasers Surg Med*. 2015;47(7):559-565. doi:10.1002/lsm.22388.
34. Boxall, Andy. The nubmer of smartphone users is expected to reach 6.1 billion by 2020. *Digital trends* . [Online] 6 3, 2015. [Cited: April 9, 2017.] https://www.digitaltrends.com/mobile/smartphone-users-number-6-1-billion-by-2020/.

35. Smith ZJ, Chu K, Espenson AR, Rahimzadeh M, Gryshuk A, et al. (2011) Cell-Phone-Based Platform for Biomedical Device Development and Education Applications. PLoS ONE 6(3): e17150. doi:10.1371/journal.pone.0017150.

36. Ch'ng, Benjamin Jin Seong, "Development of smartphone-based spectroscopy instruments for diagnostic test analysis" (2015). *Graduate Theses and Dissertations.* Paper 14778.

37. Zhang, C., Gong, C., Edwards, P., Da-Zhou, M., Zheng, S., & Liu, Z. (2015). G-Fresnel smartphone spectrometer. Lab on a Chip, 16,246.

38. Matas, A., Sowa, M. G., Taylor, V., Taylor, G., Schattka, B. J., & Mantsch, H. H. (2001). Eliminating the issue of skin color in assessment of the blanch response. Advances in Skin & Wound Care, *14*(4), 180-188.

39. J. Q. Brown, K. Vishwanath, G. M. Palmer, and N. Ramanujam, Curr. Opin. Biotechnol. 20, 119 (2009).

40. B. Chance, "Near-infrared images using continuous, phase-modulated, and pulsed light with quantitation of blood and blood oxygenation", in Advances in Optical Biopsy and Optical Mammography, R. R. Alfano, Ed. (The New York Academy of Sciences, New York, New York, p. 29.

41. T. J. Flotte, Adv. Opt. Biopsy Opt. Mammogr., Annals NY Acad. Sci. 838, 143 (1998).

42. N. S. Nishioka, Can. J. Gastroent. 17, 376 (2003).

43. M. A. Suhr, C. Hopper, L. Jones, J. G. George, S. G. Bown, and A. J. MacRobert, Int. J. Oral Maxillofacial Surg. 29, 453 (2000).

44. K. Svanberg, C. Klinteberg, A. Nilsson, I. Wang, S. Andersson-Engels, and S. Svanberg, Adv. Opt. Biopsy Opt. Mammogr., Annals NY Acad. Sci. 838, 123 (1998).

45. T. Vo-Dinh, M. Panjehpour, and B. Overholt, ''Laser-induced fluorescence for esophageal cancer and dysplasia diagnosis'', in Advances in Optical Biopsy and Optical Mammography, R. R. Alfano, Ed. (The New York Academy of Sciences, New York, 1998), p. 116.

46. G. Zonios, R. Cothren, J. M. Crawford, M. Fitzmaurice, R. Manoharan, J. Van-Dam, and M. S. Feld, Adv. Opt. Biopsy Opt. Mammogr., Annals NY Acad. Sci. 838, 108 (1998).

47. M. Chandra, J. Scheiman, D. Heidt, D. Simeone, B. McKenna, and M. A. Mycek, J. Biomed. Opt. 12, 060501 (2007).

48. M. Chandra, K. Vishwanath, G. D. Fichter, E. Liao, S. J. Hollister, and M. A. Mycek, Opt. Exp. 14, 6157 (2006).

49. Molugaram, K, Rao, S. "ANOVA (Analysis of Variance)" *Statistical techniques for transportation engineering*. 2017.451-462.Online.